Bioactive Materials 16 (2022) 388–402

Contents lists available at ScienceDirect

Bioactive Materials

journal homepage: www.keaipublishing.com/en/journals/bioactive-materials

Multi-crosslinking hydrogels with robust bio-adhesion and pro-coagulant activity for first-aid hemostasis and infected wound healing

Chen-Yu Zou [a,1], Xiong-Xin Lei [a,1], Juan-Juan Hu [a,b], Yan-Lin Jiang [a], Qian-Jin Li [a], Yu-Ting Song [a], Qing-Yi Zhang [a], Jesse Li-Ling [a,c], Hui-Qi Xie [a,*]

[a] Laboratory of Stem Cell and Tissue Engineering, Orthopedic Research Institute, Med-X Center for Materials, State Key Laboratory of Biotherapy, West China Hospital, Sichuan University, Chengdu, 610041, PR China
[b] Department of Otolaryngology, Head and Neck Surgery, West China Hospital, Sichuan University, Chengdu, 610041, PR China
[c] Department of Medical Genetics, West China Second Hospital, Sichuan University, Chengdu, 610041, PR China

ARTICLE INFO

Keywords:
Bio-adhesion
First-aid hemostasis
Infected wound healing
Polysaccharide-based hydrogel
Tannic acid

ABSTRACT

Bio-adhesive polysaccharide-based hydrogels have attracted much attention in first-aid hemostasis and wound healing for excellent biocompatibility, antibacterial property and pro-healing bioactivity. Yet, the inadequate mechanical properties and bio-adhesion limit their applications. Herein, based on dynamic covalent bonds, photo-triggered covalent bonds and hydrogen bonds, multifunctional bio-adhesive hydrogels comprising modified carboxymethyl chitosan, modified sodium alginate and tannic acid are developed. Multi-crosslinking strategy endows hydrogels with improved strength and flexibility simultaneously. Owing to cohesion enhancement strategy and self-healing ability, considerable bio-adhesion is presented by the hydrogel with a maximal adhesion strength of 162.6 kPa, 12.3-fold that of commercial fibrin glue. Based on bio-adhesion and pro-coagulant activity (e.g., the stimulative aggregation and adhesion of erythrocytes and platelets), the hydrogel reveals superior hemostatic performance in rabbit liver injury model with blood loss of 0.32 g, only 54.2% of that in fibrin glue. The healing efficiency of hydrogel for infected wounds is markedly better than commercial EGF Gel and Ag^+ Gel due to the enhanced antibacterial and antioxidant properties. Through the multi-crosslinking strategy, the hydrogels show enhanced mechanical properties, fabulous bio-adhesion, superior hemostatic performance and promoting healing ability, thereby have an appealing application value for the first-aid hemostasis and infected wound healing.

1. Introduction

Uncontrolled bleeding is a leading cause of death during war, accidents and natural disasters [1–3]. As an imperative means of emergency hemostasis, prompt wound closure can effectively reduce blood loss and increase the chance of survival [4,5]. Clinically, suture and stapling have been the standard procedures for wound closure. However, owing to the requirement of preoperative anesthesia, strict surgical requirements and time consuming, such procedures have been restricted to the operating room, especially in emergency situations [6,7]. Furthermore, the invasiveness of the operation may lead to secondary injury, wound infection and hampered wound healing, causing pain and inconvenience to the patients [8]. Accordingly, advanced wound closure strategies suitable for on-site operation and easy to use in first-aid treatment are in great demand.

By tightly adhering to the tissue surface to close the wound, bio-adhesives can dramatically change the practice of emergency treatment [9]. First-generation bio-adhesives are already available for clinical use and have shown great superiority for noninvasive wound closure [10]. Among these, fibrin glue and cyanoacrylate glue are most widely used and can effectively seal the wounds by sticking to the tissue surface. Nevertheless, several intractable features have limited their use. The fibrin glue is mainly comprised of fibrinogen, thrombin and calcium chloride. For its low adhesion strength, inadequate biosafety and high risk of infection, the fibrin glue has been confined to applications in the first-aid treatment [11]. Although with great adhesion strength,

Peer review under responsibility of KeAi Communications Co., Ltd.
* Corresponding author.
E-mail address: xiehuiqi@scu.edu.cn (H.-Q. Xie).
[1] These authors contributed equally to this work.

https://doi.org/10.1016/j.bioactmat.2022.02.034
Received 24 December 2021; Received in revised form 9 February 2022; Accepted 28 February 2022
Available online 9 March 2022

cyanoacrylate adhesives have biosafety concerns due to the presence of toxic degradation products such as formaldehyde [12]. Therefore, next-generation first-aid bio-adhesives should have the following characteristics: I) sound biocompatibility, i.e., not to trigger a strong inflammatory response; II) reliable bio-adhesion which can control the bleeding; III) ease of use, quick and easy operation for emergent situations; IV) sufficient mechanical properties to resist external impacts; V) ability to suppress bacterial growth caused by the hostile environment; VI) pro-healing properties to facilitate tissue regeneration [13–15].

Naturally derived polysaccharides have attracted great interest for excellent biocompatibility, biodegradation, inherent antibacterial property, pro-healing effect, low cost and readiness for chemical modification [16–19]. Various bio-adhesive polysaccharide-based hydrogels have been prepared through different crosslinking strategies [20]. Thereinto, dynamic covalent bonds based on the click chemistry, e.g., imine and borate ester bonds, can confer the hydrogels with self-healing, reversibility and unique mechanical properties, showing potential application value for many fields including bone fracture and diabetic wound healing [21–25]. Unfortunately, insufficient mechanical and adhesive strength have still restricted the applications of polysaccharide-based hydrogels in tissue adhesion and hemostasis. As a result, to improve their mechanical property and tissue adhesion is in urgent need [26,27]. The photocuring strategy, with the advantages of in situ curing, easy control and use, has been applied in dentistry, industrial and other fields [28–31]. As reported, many photocured hydrogels have shown excellent mechanical properties with improved stiffness and strength [32,33]. As a widely used crosslinking agent, tannic acid (TA), an FDA-approved plant-derived polyphenol, can form abundant hydrogen bonds in hydrogels and has unique bioactivities, e.g., antioxidant, antibacterial and pro-coagulant properties, with an appeal for hemostasis and wound healing [34]. Pourjavadi et al. have prepared a double-network hydrogel based on the irreversible crosslinking of polyacrylamide chains and Schiff-base reversible crosslinking. The synergistic effect has conferred the hydrogel with great strength, stretchability, rapid self-healing property, and self-adhesiveness to various materials [35]. Hence, the multi-crosslinking strategies may confer the polysaccharide-based hydrogel with sufficient mechanical properties, excellent bio-adhesion and hemostatic bioactivity.

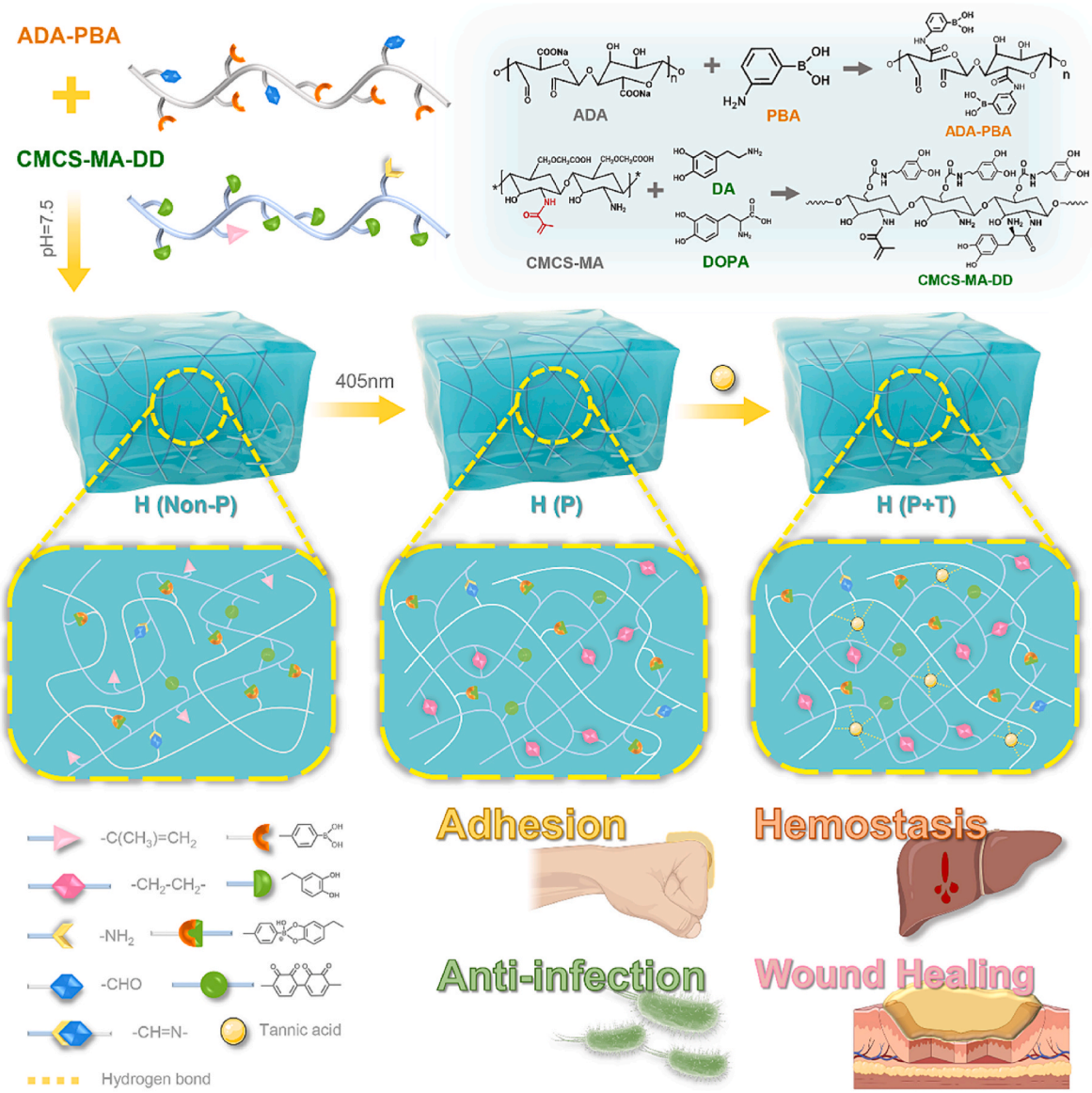

Scheme 1. Schematic representation of the multi-functional hydrogels for the first-aid hemostasis and infected wound healing. H (Non-P) was formed via dynamic covalent bonds (the borate ester bonds and Schiff base bonds); H (P) was formed via dynamic covalent bonds and photocuring excited by the 405-nm light; H (P + T) was formed via dynamic covalent bonds, photocuring excited by the 405-nm light and hydrogen bonds introduced by TA.

As a result, multifunctional bio-adhesive hydrogels, namely H (Non-P), H (P) and H (P + T), comprising carboxymethyl chitosan (CMCS), sodium alginate (SA) and TA were developed (Scheme 1). To implement the multi-crosslinking strategies, methacrylate and catechol groups were grafted into the backbone of the CMCS, and aldehyde and boronophenyl groups were grafted into the backbone of the SA. TA was added to the hydrogels. The mechanical, antibacterial and antioxidant properties of the hydrogels, in particular bio-adhesion, were further explored and optimized. *In vivo* hemostatic performance of the hydrogels was compared with that of fibrin glue in a rabbit model. Furthermore, the pro-coagulant mechanism was discussed in depth. Meanwhile, the healing effect of the hydrogels was compared with that of commercially made EGF Gel and Ag^+ Gel using an infected full-thickness skin defect model. Our results suggested that the bio-adhesive hydrogels formed through multi-crosslinking may provide a promising candidate for first-aid hemostasis and infected wound healing.

2. Experimental section

2.1. Morphology and mechanical behavior of the hydrogels

The morphology of the H (Non-P), H (P) and H (P + T) was characterized with a scanning electron microscope (SEM, EVO MA10, ZEISS, Germany). An uniaxial compression test was chosen to describe the mechanical properties of the hydrogel on a universal mechanical testing machine (Instron 5967, USA). And the compression modulus and compressive strength were further analyzed. Details are available in Supporting Information.

2.2. Swelling and degradation of the hydrogels

Swelling and degradation property of the H (Non-P), H (P) and H (P + T) were measured with the swelling ratio and weight remaining ratio, respectively. Details are available in Supporting Information.

2.3. Adhesive capability of the hydrogels

The bio-adhesion properties of the H (Non-P), H (P) and H (P + T) hydrogels were evaluated with a lap shear test and a T-peel test on a universal mechanical testing machine (Instron 5967, USA) according to modified ASTM F2255-05 and ASTM F2256-05. Adhesion of the hydrogels with various organs and pig skin was evaluated by a series of macroscopic adhesion experiments. The adhesion failure mode of the hydrogels was analyzed with tensile test. Details are available in Supporting Information.

2.4. Rheological properties and self-healing of the hydrogels

The strain amplitude sweep and alternate step strain sweep were carried out to characterize the rheological properties of the H (Non-P), H (P) and H (P + T) by using a rotational rheometer (Physica MCR302, Anton Paar, Austria). Meanwhile, to assess their macroscopic self-healing behavior, two differently dyed hydrogels were lift with a tweezer after touched together for 5 min. Moreover, the self-healing property of the H (Non-P), H (P) and H (P + T) were measured with a rotational rheometer (Physica MCR302, Anton Paar, Austria), and the self-healing efficiency of the H (P + T) at various time points (30, 60, 90, 120 min) was measured with a lap shear test as described above. A modified bursting test was used to determine the burst pressure at the initial and self-healing stages. Details are available in Supporting Information.

2.5. Biocompatibility of the hydrogels and cell migration assay

The cyto-, hemo- and histo-compatibility of the H (Non-P), H (P) and H (P + T) were evaluated with cell proliferation assay, Live/Dead staining, hemolysis assay and subcutaneous implantation, respectively. All animal experiments were approved by Sichuan University Animal Care and Use Committee and carried out in accordance with the relevant principles (No.20211481A). Human skin fibroblasts (HSF cells) were employed for the measurement of cell migration. Details are available in Supporting Information.

2.6. Antibacterial capability of the hydrogels

Gram-positive *S. aureus* (ATCC 6538) and gram-negative *E. coli* (ATCC 25922) were used for evaluating the antibacterial properties of the H (P) and H (P + T). The bacterial viability after different treatments was evaluated. And the morphology of *S. aureus* and *E. coli* was observed by SEM. The Details are available in Supporting Information.

2.7. Antioxidant capability of the hydrogels

The antioxidant properties of the H (Non-P), H (P) and H (P + T) were first demonstrated by scavenging stable free radicals ($DPPH^{\bullet}$ and $PTIO^{\bullet}$). At the cellular level, excessive oxidative stress model of the NIH-3T3 cells was constructed for determining the antioxidant ability of the hydrogel. Details are available in Supporting Information.

2.8. In vitro pro-coagulant properties of the hydrogels

Commercially made fibrin glue (Guangzhou Bioseal Biotech Co., Ltd., China) was used as the control in the follow-up experiments. The *in vitro* hemostasis ability of the H (Non-P), H (P) and H (P + T) was verified by the coagulation time of whole blood and blood clotting index (BCI) assay. The adherent platelets on the surface of the H (P), H (P + T) and fibrin glue were quantified with a lactate dehydrogenase (LDH) assay kit (Nanjing Jiancheng Bioengineering Institute, Nanjing, China). Furthermore, the morphology of the platelets and erythrocytes on the sample surface was observed by SEM after critical point drying and gold sputtering treatment. Details are available in Supporting Information.

2.9. In vivo hemostasis properties of the hydrogels

The *in vivo* hemostatic performance of the H (P) and H (P + T) was assessed with the rabbit model for liver injury. Commercially made fibrin glue was used as the control. Male New Zealand white rabbits (weighing 2.5–3.0 kg) were anesthetized with pentobarbital sodium (1.1 mL kg^{-1}) and placed in supine position. A 10-cm-long incision was made in the abdomen for the exposure of the liver. After drying excess fluid and blood with gauze, the liver leaf was carefully placed on a pre-weighed filter paper. Bleeding was caused by making a 5-mm-long and 2-mm-deep incision on the liver surface with a scalpel. Thereafter, pre-formed hydrogel was covered on the wound, followed by illumination for 60 s (405 nm, 25 mW cm^{-2}). The bleeding time was recorded with a stopwatch, and blood loss was determined by weighing the filter paper beneath the liver leaf after 5 min. All experiments were repeated for five times.

2.10. Wound healing in a model for infected full-thickness skin defect

Male Sprague-Dawley (SD) rats (weighing 200–250 g each) were used for constructing the model for infected full-thickness skin defect. The rats were divided into PBS group, EGF Gel group, Ag^+ Gel group, H (P) group and H (P + T) group, with 3 rats for each group at each time point. PBS was used as the negative control, and two types of commercially made gels containing epidermal growth factor (EGF) [50,000 IU (100 μg)/10 g] and Ag^+ [750–1050 μg/g (w/w)] purchased from Guilin Pavay Gene Pharmaceutical Co., Ltd. and Shenzhen Yuanxing Pharmaceutical Co., Ltd. in China, respectively, were used as the positive controls. Wound healing was observed and photographed at 3, 7, 14 and 21 days. 400 μL of fresh hydrogel was replaced at the same time.

Details are available in Supporting Information.

2.11. Histological analysis

The level of oxidative stress was determined with a dihydroethidium (DHE) probe by using a frozen section ROS detection kit (Beijing Biorab Technology Co., Ltd., China) after various treatments, and the mean fluorescence intensity was analyzed by using Image J (n = 3). Fixed tissue was embedded in paraffin and sectioned into 4-μm-thick slices. H&E staining, Masson staining and Sirius red staining were carried out by following the manufacturer's instructions. The thickness of the epithelium, granulation tissue and total collagen content, and the ratio of type I to type III collagen (COL I/COL III) in the regeneration area were analyzed (n = 3). The content of TNF-α and VEGF in the wound repair area was determined with an enzyme-linked immunosorbent assay (Shanghai Zcibio Technology Co., Ltd., China). Details are available in the Supporting Information.

2.12. Statistical analysis

All data was presented as mean ± standard deviation. Statistical significance between the results was determined by one-way ANOVA and Student's t-test. $P < 0.05$ was considered to be statistically significant ($^{*}P < 0.05$, $^{**}P < 0.01$, $^{***}P < 0.001$, $^{****}P < 0.0001$).

3. Results and discussion

3.1. Preparation and characterization of the hydrogels

CMCS-MA-DD and ADA-PBA were first synthesized through a multi-step modification to prepare a hydrogel with bio-adhesive, antibacterial, antioxidant and self-healing properties. In CMCS-MA-DD, the C═C bonds were introduced to the CMCS via grafting the methacrylate groups determined by proton nuclear magnetic resonance (^{1}H NMR) spectrum (Fig. S1a). The peaks (δ = 6.62, 6.71 and 6.78 ppm) in the ^{1}H NMR spectrum and absorption peaks of amide bonds (1617 and 1539 cm^{-1}) in the Fourier transform infrared (FTIR) spectrum of CMCS-MA-DD (Figs. S1a and b) both confirmed that the catechol groups were successfully grafted. For ADA-PBA, as demonstrated by FTIR spectrum (Fig. S1b), the peak at 1734 cm^{-1} was attributed to the –CHO bonds, suggesting that the synthesis of ADA was successful. Subsequently, via classical EDC/NHS chemistry, ADA was successfully modified by the boronophenyl groups, which was proven by ^{1}H NMR and FTIR spectrum (Figs. S1a and b).

The hydrogel was formed on the strength of multi-crosslinking mechanisms. Two types of covalent bond networks were introduced into the hydrogel network, endowing it with characteristic mechanical properties. The first was the dynamic covalent bonds network produced from the borate ester bonds and Schiff base bonds. The other was the photo-triggered covalent bonds network, formed via the illumination of 405 nm light. The C═C bonds in the methacrylate group can undergo free radical polymerization to form the C–C bonds. Furthermore, the addition of TA has enhanced the hydrogel network mainly via hydrogen bonds [36]. The dynamic and photo-triggered covalent bonds formed in the hydrogel were validated via FTIR and X-ray photoelectron spectroscopy (XPS). As shown in Fig. S1b, the proportion of C═C bonds with stretching vibration, as shown by the absorption peak at 1652 cm^{-1}, was significantly higher in H (Non-P) (14.12%) than H (P) (6.32%) and H (P + T) (9.17%), confirming the generation of free radical polymerization which was excitable by the 405 nm light. In the FTIR spectra of the H (Non-P), H (P) and H (P + T), a strong absorption peak occurred at 1601 cm^{-1} ascribed to the presence of the C═N bonds, whilst the absorption peak at 1732 cm^{-1} corresponding to the stretching vibration of the C═O bonds was absent. On the other hand, as shown in Fig. S1c, the peak at 401.7 eV in N 1s spectrum was assigned to the C═N bonds, indicating the formation of Schiff base bonds. As demonstrated in O 1s spectrum, a typical peak corresponding to the B–O bonds has confirmed the formation of borate ester bond.

The optimal concentration of the two components in the hydrogel was determined by rheological testing based on the control variates. As shown in Fig. S2, along with the increase of ADA-PBA concentration, the storage modulus (G') and strain corresponding to the flow point (τ_f) of the hydrogel have shown an increasing trend before and after photocuring. As a result, the optimal concentration of ADA-PBA was determined as 10%. Nevertheless, with a constant concentration of ADA-PBA (10%), the τ_f has decreased from 102.0 ± 7.9% to 83.2 ± 5.7% with the concentration of CMCS-MA-DD increased from 6% to 10% after photocuring owning to the formation of more rigid covalent bonds (the C–C bonds). By comprehensive analysis, the optimal concentrations of ADA-PBA and CMCS-MA-DD in the hydrogel were both determined to be 10%.

3.2. Physical properties of the hydrogels

As shown in Fig. 1a, c, under scanning electron microscopy (SEM), all hydrogels have revealed a porous morphology, with the average pore diameter of 89.1 ± 13.3 μm, 63.5 ± 11.0 μm and 53.7 ± 7.8 μm for the H (Non-P), H (P) and H (P + T), respectively. The H (Non-P) has the largest pore diameter among all groups, indicating the lowest degree of crosslinking. For the H (P), after further photocuring, dual-crosslinking network (C–C bonds network and dynamic covalent bonds network) have formed and the crosslinking degree was enhanced, showing decreased pore diameter. The introduction of TA in the H (P + T), which has the smallest pore diameter, has imparted the hydrogels with hydrogen bonds interactions to form multi-crosslinking networks. Additionally, energy dispersive spectrometer (EDS) detected the uniform distribution of C, O, N and B elements in the hydrogel (Figs. 1b and S3). The swelling and degradation behaviors of the hydrogels are vital for absorbing tissue exudation, maintaining hydrogel stability and tissue regeneration [37]. As shown by the swelling curve, the H (P + T) reached a swelling equilibrium of 28.3 ± 4.1% after 30 h, while the mass of the H (Non-P) and H (P) began to decline with the incubation time, which is attributed to the destruction of the hydrogel network. Similar to swelling, the H (P + T) demonstrated the suitable degradation rate, and the remaining mass was 58.3 ± 6.1%, showing a long-term stability in PBS (Fig. 1d, e and S4). Compared with the H (Non-P) and H (P), the high crosslinking density in the H (P + T) enabled it to have a low swelling rate and moderate degradation rate, which are conducive to its stability during wound and tissue regeneration.

The mechanical properties of the hydrogels were characterized with the uniaxial compression experiment. Fig. 1f presented the stress-strain curves of the H (Non-P), H (P) and H (P + T). Owing to the flexibility and deformability of the dynamic covalent bond network, no fracture occurred during the compression depicted in Fig. S5. The mechanical properties of the hydrogels were further uncovered with compression modulus and compressive strength (Fig. 1g and h). The compression modulus of the H (Non-P), H (P) and H (P + T), which reflects their resistance to deformation, was 15.5 ± 1.2 kPa, 29.7 ± 2.1 kPa and 40.6 ± 3.9 kPa, respectively. After photocuring, the compressive strength of the hydrogels has increased from 53.0 ± 3.8 kPa to 74.7 ± 3.3 kPa. Furthermore, the strength of the H (P + T) has reached 84.5 ± 4.9 kPa after the addition of TA. In other words, the hydrogels have increased their strength while maintained the initial flexibility, which to some extent has improved the mechanical properties of polysaccharide-based hydrogels. This results from the synergistic enhancement of multiple networks of the H (P + T): In the compression process, the borate ester bonds and Schiff base bonds can be deformed and reconstructed to protect the hydrogels from destruction. The C–C covalent bonds network triggered by photocuring has provided a rigid skeleton to resist external deformation, whilst the hydrogen bonds contributed by the TA have further strengthened the network.

As essential properties of the hydrogels, the storage modulus (G′),

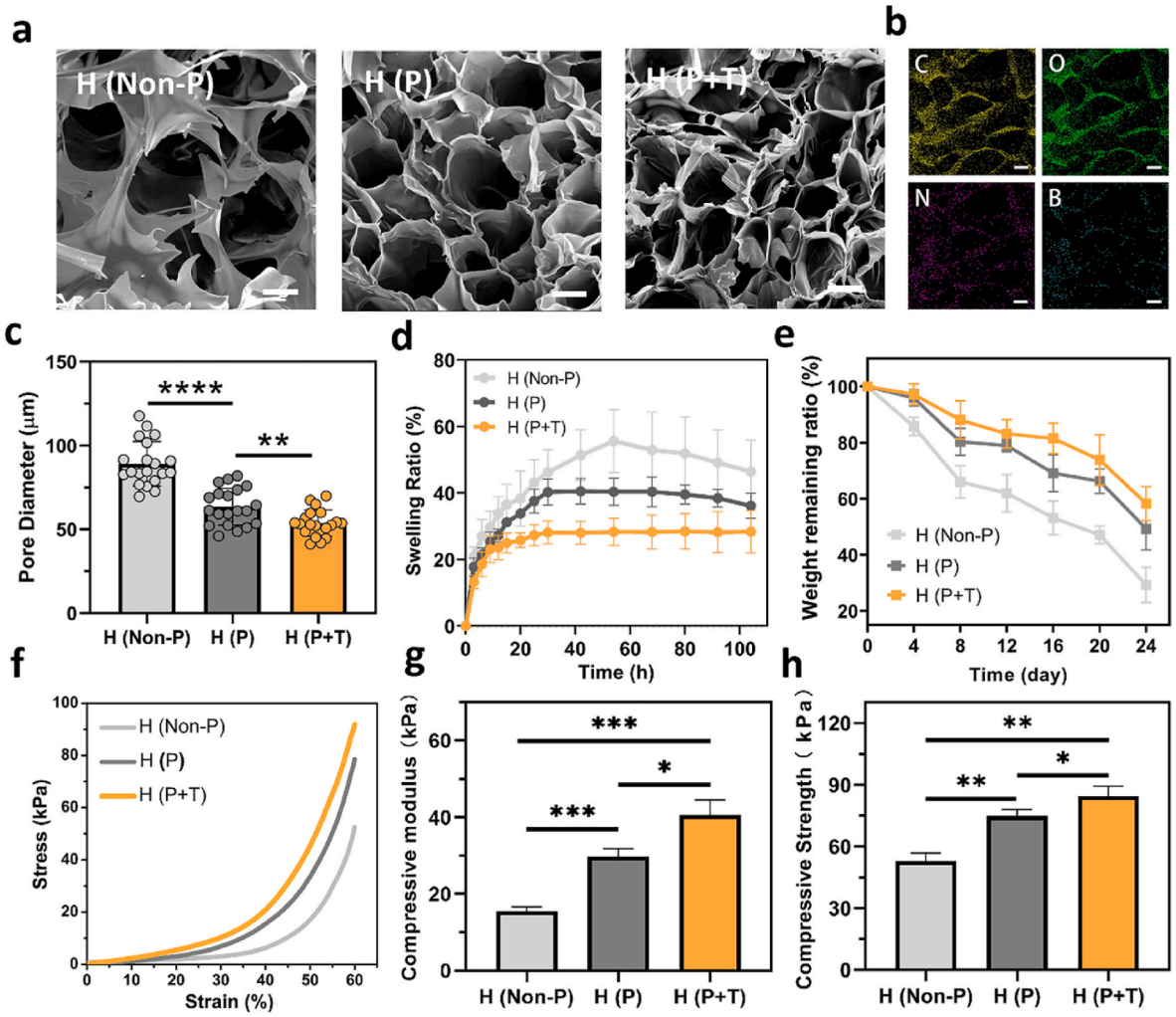

Fig. 1. a) SEM images, b) distribution of elements (C, N, O, B) and c) pore diameter of the lyophilized H (Non-P), H (P) and H (P + T), Scale bar = 200 μm; d) The swelling curves and e) degradation curves of the hydrogels; f) Stress-strain curves (60% compression rate), g) compression modulus and h) compression strength of the hydrogels (*$P < 0.05$, **$P < 0.01$, ***$P < 0.001$).

loss modulus (G″) and strain at the flow point (τ_f) were evaluated by rheological tests (Fig. S6). The results revealed that the hydrogels comprised of various crosslinking networks had different rheological properties. For the H (P + T), the G′ and τ_f are 5400.9 ± 171.7 Pa and 85.4 ± 8.2%, respectively, which have indicated excellent elasticity and flexibility.

3.3. Bio-adhesive and self-healing properties of the hydrogels

As one of the most important properties of tissue adhesives [38], bio-adhesion was evaluated by objective and intuitive tests. As shown in Fig. 2a and b, the adhesive strength and interfacial toughness of the hydrogels, as key indicators of adhesion properties, were measured by lap shear test and T-peel test. The H (Non-P), H (P) and H (P + T) showed preeminent adhesive property, with their adhesive strength being 58.2 ± 7.4 kPa, 103.2 ± 7.8 kPa and 162.6 ± 7.0 kPa, respectively, which have notably rivaled that of fibrin glue (13.2 ± 4.9 kPa). Therein, the adhesive strength of the H (P + T) was 12.3 times that of fibrin glue. Analogously, the interfacial toughness of the H (Non-P), H (P) and H (P + T), namely the energy required for interfacial crack propagation, was superior to that of the fibrin glue. The interface toughness of the H (P + T) was up to 170.7 ± 16.7 J m^{-2}, 3.3 times that of the fibrin glue (52.3 ± 2.8 J m^{-2}). Taken together, compared with the fibrin glue, the H (Non-P), H (P) and H (P + T) had better bio-adhesion properties. As presented in Fig. S7, the hydrogel was capable of bonding to major organs including the heart, stomach, kidney, rib and lung without falling out under gravity, confirming their potential use in a wide range of clinical scenarios.

Pig skin adhesion test was carried out to further characterize the adhesion and persistence of the hydrogels. Herein, the H (Non-P), H (P) and H (P + T) groups were immersed in PBS for 48 h to simulate the hostile wet environment. Before soaking, the hydrogel was sticked firmly to the skin and subjected to stretching, twisting and bending. Surprisingly, the H (P + T) has maintained good adhesion even under water currents (Movie S1). As shown in Figs. 2c and S8, the H (Non-P) and H (P) had dropped from the pig skin after soaking for 24 h and 48 h, respectively, whereas the H (P + T) still sticked strongly to the skin. The H (P + T) not only has remained attaching to the skin, but could be stretched, bent and twisted without shedding after 48 h. Furthermore, as observed under the SEM (Fig. 2d), the H (P + T) was tightly attached to the pig skin with no gap between the hydrogel and pig skin. The superb bio-adhesion and stability properties of the hydrogel result from many factors. First of all, as inspired by the strong adhesion of mussels [39,40], introduction of the catechol and boronophenyl groups into the polymer has laid the foundation for the bio-adhesion ability of the hydrogels. The hydroxyl groups of the catechol and boronophenyl groups form covalent bonds with various nucleophiles, e.g., amino or thiol groups, on the tissue through Michael addition reactions and non-covalent bonds such

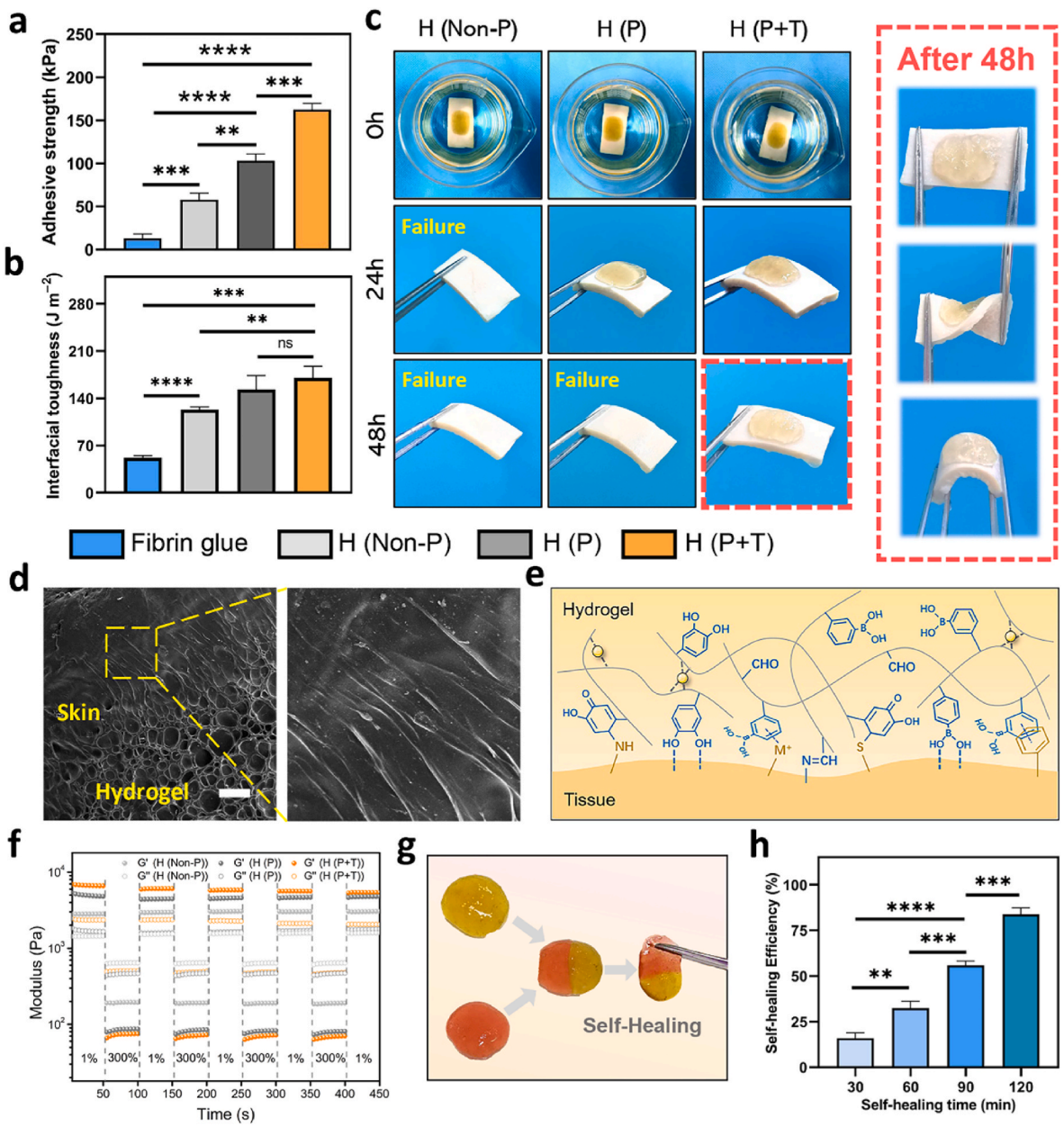

Fig. 2. a) The lap shear strength and b) interfacial toughness of the H (Non-P), H (P) and H (P + T); c) Pig skin adhesion test and bio-adhesion performance of the hydrogels after 48-h soaking; d) SEM images of the adhesive interface between the H (P + T) and pig skin, Scale bar = 200 μm; e) Schematic diagram of the adhesion between the hydrogel and tissue; f) The rheological curves of the hydrogels under alternate step strain sweep mode; g) Self-healing property of the two dyed H (P + T); h) Self-healing efficiency of the H (P + T) at various time points (**$P < 0.01$, ***$P < 0.001$, ****$P < 0.0001$, ns: no significant difference).

as hydrogen bonds. The benzene ring also interact with metal ions and benzene ring in the tissue through cation-π and π-π stacking interactions, and the remaining aldehyde groups in the hydrogels have interacted with the amino group on the tissue via Schiff base reaction (Fig. 2e). Secondly, the enhanced cohesion of the hydrogel can change the pattern of adhesion failure, which was proven by the tensile test (Figs. S9a and b). Adhesion failure has occurred inside the hydrogel (cohesion failure mode), at the adhesive interface (adhesion failure mode) or both (cohesion/adhesion failure mode) (Fig. S9c) [13,41]. To some extent, the cohesive failure caused by inadequate cohesion hinder the performance of bio-adhesion. As shown in Fig. S9d, most of the failures in H (Non-P) have occurred inside the hydrogel matrix, while in H (P) and H (P + T), they have mainly occurred at the tissue-hydrogel interface, indicating a transition from cohesion failure mode to cohesion/adhesion failure mode. Therefore, to improve the cohesion of adhesive matrix has been identified as a practical way to optimize the bio-adhesion. As confirmed by aforementioned studies, the robust C–C bonds network act as a skeleton of the hydrogels and can be interpenetrated by the flexible dynamic covalent bond network, greatly enhancing the cohesion of hydrogel, to confer it with remarkable adhesion properties. Last but not the least, for its richness in phenolic hydroxyl groups, the TA has played a dual role in the promotion of bio-adhesion. A large number of hydroxyl groups confer the TA with its own adhesion. On the other hand, the TA act as a crosslinker to further strengthen the multi-crosslinking network via the hydrogen bonds.

The concentration and adhesive strength of the hydrogel were compared with those of recently developed hydrogel adhesives (Fig. S10a). In general, the hydrogels with higher concentrations required less curing time and showed better mechanical properties, e.g., bio-adhesion. Nevertheless, the high concentration of the hydrogels was

not conducive to the injectability and mixing, and may trigger excessive immune response. Therefore, the concentration of the hydrogels should be taken into account in the pursuit of excellent bio-adhesion [6]. Compared with others, the H (Non-P), H (P) and H (P + T) showed prominent bio-adhesion (from 58.2 ± 7.4 to 162.6 ± 7.0 kPa) with an appropriate concentration (10%). As shown in Fig. S10b, the adhesive strength of the hydrogel in general has increased along with the decrease in its pore size, which may in part be attributed to the increase in its crosslinking density, i.e., the cohesion enhancement [17]. As illustrated by Tang et al. the optimal cohesiveness of the hydrogel may enhance its bio-adhesion, with the adhesive strength of GelDex-5%AMBGN being 108.48 ± 8.45 kPa [23]. Introduction of multiple hydrogel network is another important reason for the improved crosslinking density and bio-adhesion. Teng et al. have developed a series of V-Gel hydrogels. By adjusting the concentration of the hydrogels, the pore diameter of the V-Gels has decreased from 16.7 ± 2.2 to 10.6 ± 1.4 μm owing to the enhanced crosslinking density. Furthermore, owning to the dynamic Fe^{3+}-catechol complexes, the R-Gels also showed greater adhesive strength compared with the V-Gels at the same concentration [10]. Taken together, the above analysis has demonstrated that improvement of the cohesion and adjustment of the crosslinking strategy can effectively improve the bio-adhesion of the hydrogels.

Considering its pivotal role in the self-healing behavior of the tissue adhesive, particularly at the site of large deformation, the self-healing behavior of the hydrogels was comprehensively explored. As depicted in Fig. 2f, the hydrogel network was destroyed ($G' < G''$) at a high strain (300%), but has remained intact ($G' > G''$) at a low strain (1%). When the oscillatory strain was switched back and forth between 1% and 300%, the hydrogels also changed between reconstruction and destruction, suggesting that the hydrogels were able to self-heal. In Fig. 2g, after contact for 5 min, two dyed hydrogels could be picked up with tweezers and stretched (Movie S2). The damaged interface was reconnected owing to the immediate recombination of the borate ester bond and Schiff base bond. Moreover, the self-healing efficiency at various time points was evaluated with a lap shear test (Figs. 2h and S11). After 120 min of self-healing, the adhesive strength of the H (P + T) has reached 131.4 ± 5.9 kPa, which was equivalent to 83.8 ± 3.6% before the destruction (162.6 ± 7.0 kPa). That said, the self-healing efficiency has reached 83.8 ± 3.6%. On the other hand, the fibrin glue needs to be changed once broken, as it is devoid of the capability of reintegration, resulting in waste and high cost. By comparison, the H (P + T) showed not only better adhesion performance but also self-healing properties. Furthermore, as shown by the bursting test (Fig. S12c), the burst pressure of H (P + T) was 130.3 ± 4.4 mmHg, which was significantly higher than that of the fibrin glue, H (Non-P) and H (P) ($P < 0.05$). Notably, this was also remarkably higher than the normal systolic blood pressure (120 mmHg), making it more efficient for *in vivo* applications [42]. As confirmed by previous studies, through multi-crosslinking, the H (P + T) could attain the optimal bio-adhesion and cohesion, which has conferred a resistance to the blood pressure. To illustrate the role of self-healing in blood pressure resistance, a bursting test was carried out after various times of self-healing (30 and 60 min). As shown in Fig. S12d, the burst pressure of the H (P + T) at the initial and self-healing stages (60 min) showed no significant difference ($P > 0.05$). That said, should the hydrogel be damaged by external stress, the network can be reconstructed timely to recover its integrity, and the adhesive strength is restored at large, which is beneficial to the sealing effect of the hydrogels and prevention of bacterial invasion.

3.4. Antibacterial and antioxidant properties of the hydrogels

As one of the most common and intractable problems in clinical practice, wound infection can seriously threaten the health of patients, in particular those under harsh conditions [43]. Aberrant reactive oxygen species (ROS) produced by excessive oxidative stress impedes the healing of infected wounds [25,44]. Apart from providing a moist environment, the hydrogels should also have antibacterial and antioxidant properties upon clinical application. As an effective antibacterial drug, ampicillin was used as the positive control. As shown in Fig. 3a and b, after contacting *Escherichia coli* (*E. coli*) and *Staphylococcus aureus* (*S. aureus*) directly with the hydrogel for 4 h, fewer colonies were found in the H (P), H (P + T) and ampicillin groups compared with the PBS group. As confirmed by statistical analysis, ampicillin demonstrated a remarkable antibacterial effect for gram-negative *E. coli*, and the bacterial viability was only 1.9 ± 1.0%. The viability of the bacteria in the H (P) and H (P + T) groups was 24.3 ± 3.3% and 7.4 ± 3.1%, respectively, both denoting effective inhibition for the growth of *E. coli*. The H (P), H (P + T) and ampicillin groups also showed antibacterial effect against gram-positive *S. aureus*, with the bacteria viability being 6.6 ± 0.3%, 4.0 ± 1.4% and 2.3 ± 1.6%, respectively. Moreover, as shown in Fig. S13, the bacterial wall of *E. coli* and *S. aureus* treated by H (P) and H (P + T) appeared to shrink, indicating the structure is damaged and bacterial activity is affected. The excellent resistance of the hydrogel to *E. coli* and *S. aureus* have involved adhesion and destruction of the bacteria. The bacteria were first trapped by the residual phenolic hydroxyl groups and protonated amino groups in the hydrogel. Thereafter, the protonated amino groups in the CMCS and quinone groups formed by oxidation of the catechol groups interacted with the bacterial wall, causing dysfunction and even destruction of the bacterial membrane [45]. The introduction of the TA has enabled the hydrogel to destroy the structure of bacterial wall to improve its antibacterial effect. He et al. have synthesized a series of TA-reinforced hydrogels, which showed significantly enhanced antibacterial effect, and the inhibition rate of bacterial growth was TA concentration-dependent [46]. Notably, the antibacterial effect of the hydrogel was more pronounced on gram-positive *S. aureus*. As proposed, one possibility was that the TA can directly bind to the peptidoglycan on the wall of gram-positive bacteria, whilst the outer lipid membrane of gram-negative bacteria can prevent such binding. Secondly, the positive charges of the hydrogels conferred by the protonated amino groups stick firmly with the negatively charged gram-positive bacteria owning to the teichoic acid in the cell wall, which is absent in gram-negative bacteria, causing inadequate adhesion to the hydrogel [47]. For their natural origin, both CMCS and TA have inherent antibacterial properties to prevent the resistance caused by antibiotics to some extent [48].

The antioxidation property of the H (Non-P), H (P) and H (P + T) groups was evaluated by $DPPH^{\bullet}$ and $PTIO^{\bullet}$, the stable nitrogen-centered and oxygen-centered radical, respectively. For the $DPPH^{\bullet}$ test (Fig. 3c), the H (Non-P), H (P) and H (P + T) have all shown remarkable efficiency for free radical scavenging, with the $DPPH^{\bullet}$ exceeding 75% and H (P + T) as high as 92.2 ± 2.9%, albeit with no significant difference from the TA solution (positive control) ($P > 0.05$). Similarly, as shown in Fig. 3d, the $PTIO^{\bullet}$ scavenging of the H (Non-P), H (P) and H (P + T) was 76.4 ± 1.0%, 74.7 ± 8.9% and 86.7 ± 3.7%, respectively. After various treatments, the $DPPH^{\bullet}$ and $PTIO^{\bullet}$ solution were photographed, respectively, with residual free radicals characterized by electron paramagnetic resonance (EPR, Fig. S14). To verify the ROS scavenging ability of the hydrogel at the cellular level, a model of oxidative stress was constructed with the NIH-3T3 cells using H_2O_2, and the ROS level was determined by using a DCFH-DA probe. As confirmed by flow cytometry (Figs. 3e and S15), the extracellular ROS level was drastically different after various treatments. As a recognized antioxidant and the positive control, the TA showed the best ROS scavenging effect with a positive rate of 17.3 ± 3.9%. The positive rate was 25.5 ± 4.1% when treated by H (P + T), which was significantly lower than after the H (Non-P) and H (P) treatment (37.7 ± 4.1% and 42.4 ± 6.1%, respectively). Analogously, as shown in Fig. 3f and g, the reduction of DCFH-DA fluorescence intensity has indicated a significant ROS scavenging effect induced by the hydrogels, in particular the H (P + T). The excellent antioxidant capacity of the hydrogels is attributable to the large number of reductive hydroxyl groups present in the catechol groups, boronophenyl groups and TA, as the hydrogen atoms in the hydroxyl groups tend to dissociate

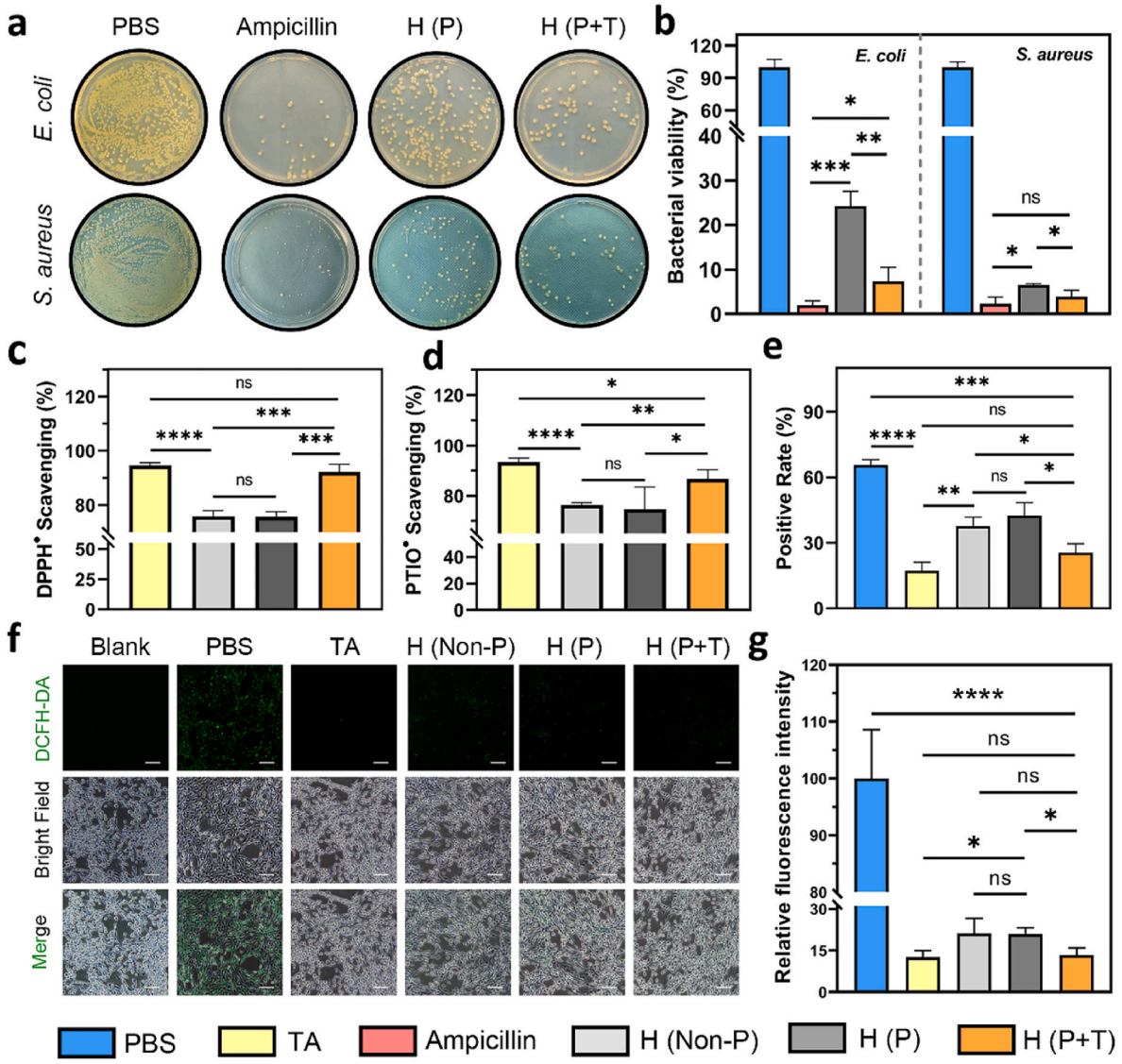

Fig. 3. a) Survival and b) viability of *E. coli* and *S. aureus* after PBS, H (P), H (P + T) and ampicillin treatment; The c) DPPH• and d) PTIO• scavenging efficiency of various groups; e) DCFH-DA positive rate of various groups analyzed by flow cytometric; f) DCFH-DA fluorescence images and g) fluorescence intensity after various treatments, Scale bar = 200 μm (*$P < 0.05$, **$P < 0.01$, ***$P < 0.001$, ****$P < 0.0001$, ns: no significant difference).

into protons caused by the increased polarity of the hydroxyl groups [49].

3.5. *In vitro and in vivo* biocompatibility of the hydrogels

As the most essential characteristics, cyto-, hemo- and histocompatibility play a pivotal role in the research of biomaterials. As demonstrated by the CCK-8 assay, the proliferation of the NIH-3T3 cells in the extract of the H (Non-P), H (P) and H (P + T) was not affected compared with the complete medium (Fig. 4a), suggesting that the hydrogel contained no obvious cytotoxic ingredient. Live/Dead fluorescence images (Fig. 4b) indicated that the NIH-3T3 cells grew normally in all three hydrogel extracts, with a spindle shape and few dead cells (red area). Furthermore, as shown by the hemolysis test, the H (Non-P), H (P) and H (P + T) all had excellent hemocompatibility, with no rupture occurring after the contact with the hydrogels, with the hemolysis rate being less than 5% (Fig. 4c). Upon cell migration experiment (Fig. 4d and e), the HSF cells have migrated to the blank area with the elapse of time, with the migration rate (at 48 h) induced by the H (P + T) (83.5 ± 1.6%) being significantly higher than by the complete medium (52.0 ± 5.9%). This is because the polysaccharides in the hydrogel are conducive to fibroblast recruitment which is beneficial for wound healing.

Histocompatibility is another important indicator for the evaluation of biocompatibility, which also reflect the reaction between the implant and the host. To investigate this, the hydrogel was embedded subcutaneously. As shown by the gross view in Fig. 5a and b, no obvious signs of tissue necrosis, hyperemia and purulency were noted in the subcutaneously implanted area of the hydrogels at 7, 14 and 21 days, and the volume of all hydrogels was significantly reduced over time, denoting their biodegradability *in vivo*. Moreover, a layer of tissue was found to surround the H (P + T), which was difficult to separate, indicating that the hydrogel has well integrated with the tissue. The remainder mass of the H (Non-P), H (P) and H (P + T) was counted in Fig. 5c. The H (P + T) showed a reasonable degradation rate among the three groups, with the remainder mass of 41.8 ± 3.2% after 21 days, while the H (Non-P) was only 5.5 ± 2.8% due to the fast degradation rate. The degradation rate of the hydrogels mainly depends on the degree of crosslinking. Notably, the H (P + T) with multi-crosslinking networks comprised of dynamic covalent bonds, C–C covalent bonds and hydrogen bonds have the highest

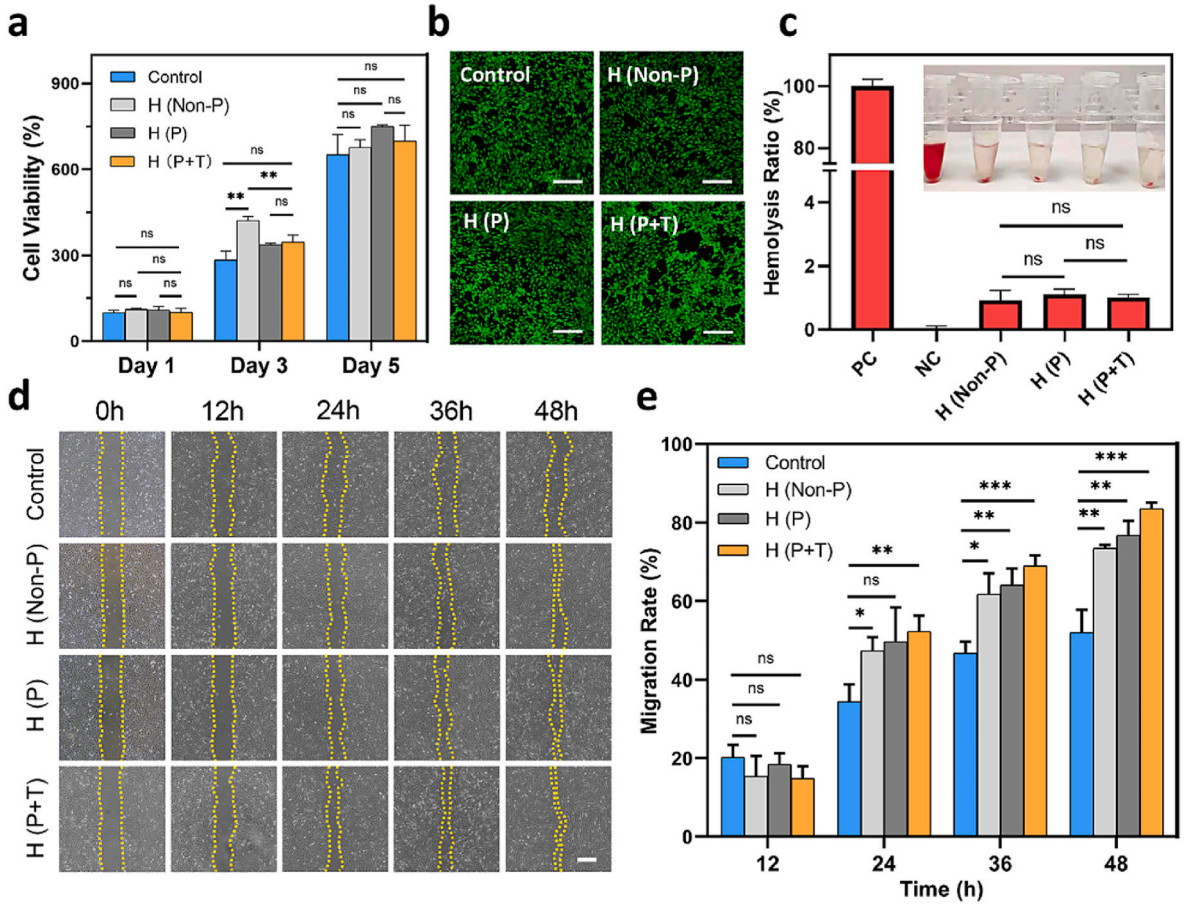

Fig. 4. a) The effects of the H (Non-P), H (P) and H (P + T) on the proliferation of the NIH-3T3 cells; b) Live/Dead staining fluorescence images of various groups after incubation with the abstract for 3 days, Scale bar = 200 μm; c) Hemolysis ratio of the hydrogels (PC: 0.1% Triton X-100, NC: PBS); d) The images and e) migration rate of the HSF cells treated with the hydrogels, Scale bar = 200 μm (*$P < 0.05$, **$P < 0.01$, ***$P < 0.001$, ns: no significant difference).

crosslinking density and hold greater promises for clinical applications, which can better maintain the shape even in the presence of various enzymes and body fluids *in vivo*.

H&E staining and immunofluorescence staining of CD86 were conducted to further evaluate the hydrogel-host interactions (Figs. 5d and S16). Shortly after the subcutaneous implantation (within 7 days), a large number of cells, mainly inflammatory cells, had infiltrated into the hydrogels, indicating that they have caused a typical inflammatory response. Various subtypes of macrophages play different roles in inflammation, among which the role of M1-type macrophages is to intensify the inflammatory response [50,51]. As verified by CD86 immunofluorescence staining, the number of M1-type macrophages had decreased over time, suggesting that the degradation products of the hydrogel did not exacerbate the inflammatory response. Additionally, as the material degraded, due to the recruitment of fibroblasts, nascent connected tissue was generated around the hydrogel instead of forming capsule layer, indicating synchronous formation of new tissue and degradation of the hydrogels. It is worth noting that the degradation of the hydrogels is contributed to the regeneration of granulation tissue which is essential for wound healing [32,52]. Furthermore, H&E staining revealed that the 21-day implantation of the H (Non-P), H (P) and H (P + T) caused no significant pathological changes in major organs including the heart, liver, spleen, lung and kidney (Fig. S17). The results of routine blood tests and biochemistry assays have found that the kidney and liver functions were normal compared with those of healthy rats (Fig. S18). Collectively, the *in vitro* and *in vivo* evaluations showed that the hydrogels have excellent biocompatibility and are safe enough for further *in vivo* experiments.

3.6. *In vitro pro-coagulant and in vivo hemostatic performance of the hydrogels*

Uncontrolled bleeding during wartime and accidents is a great concern for medical care worldwide. Hence, effective control of bleeding is indispensable for tissue adhesives. To evaluate the pro-coagulant rate of the hydrogels *in vitro*, the coagulation time of whole blood and blood clotting index (BCI) were first determined. In Fig. 6a, compared with the blank group (833.3 ± 112.5 s), the rate of blood clot formation induced by the H (Non-P) and H (P) and H (P + T) was significantly increased with the coagulation time being 493.7 ± 24.1 s, 476.7 ± 74.8 s and 324.7 ± 36.6 s, respectively. The fibrin glue (positive control) was not significantly different from the H (P + T) ($P > 0.05$). Among the three hydrogels, the H (P + T) showed the lowest BCI for only 32.1 ± 4.7%, while the H (Non-P) and H (P) were 49.0 ± 4.9% and 46.2 ± 5.5%, respectively (Fig. 6b). Since a lower BCI value implies a higher rate of blood clot formation, coagulation was initiated earlier by the H (P + T), possibly due to addition of the TA.

To explore the underlying mechanism of their pro-coagulant effect, the interaction between the hydrogels and the main cells in the blood was further investigated. Platelets are of prime importance in hemostasis during the clotting process. In the present study, adherent platelets on the hydrogel surface were quantified with LDH assay kits as listed in Figs. 6c and S19. As the adhesion time increased from 5 min to 60 min, the number of adherent platelets showed exponential increases in the fibrin glue, H (P) and H (P + T) groups. The adhesion capacity of the H (P + T) to the platelets ($4.6 \times 10^7 \pm 4.1 \times 10^6$) was remarkably greater than the H (P) ($3.2 \times 10^7 \pm 1.0 \times 10^6$), with the number of adherent

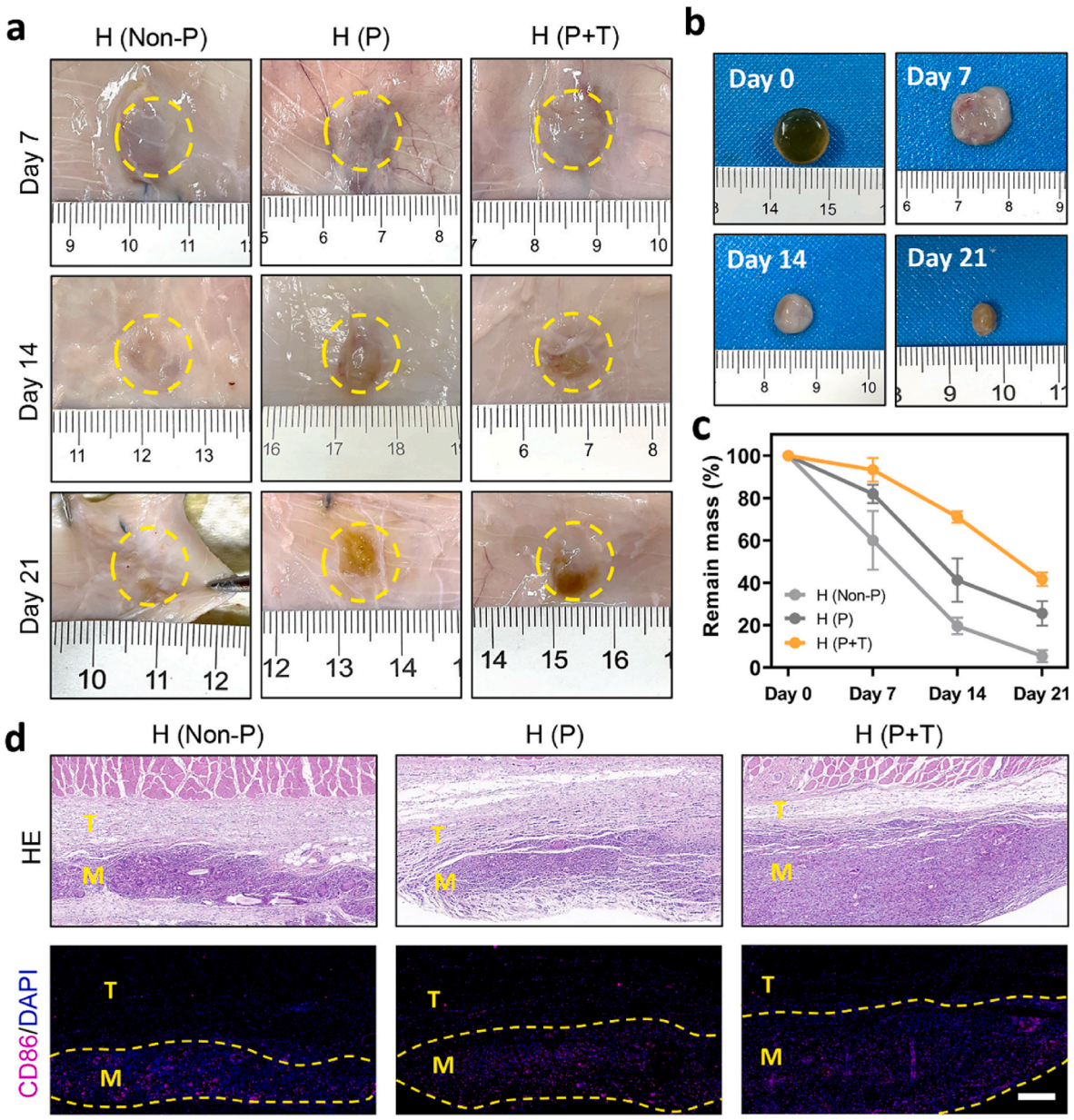

Fig. 5. a) Gross appearance of the H (Non-P), H (P) and H (P + T) groups after 7, 14 and 21 days of subcutaneous implantation; b) Gross appearance of the H (P + T) before and after 7, 14 and 21 days; c) The curves for remained masses of the hydrogels during subcutaneous implantation; d) H&E staining and immunofluorescence staining of CD86 after 21 days' implantation of the hydrogels, Scale bar = 200 μm (T: tissue, M: material, CD86 labeled M1-type macrophages, DAPI labeled nuclei). (For interpretation of the references to colour in this figure legend, the reader is referred to the Web version of this article.)

platelets on the surface of H (P + T) being 1.4 times that of the H (P) after 60 min of incubation. Moreover, the difference between the number of platelets on the fibrin glue ($4.6 \times 10^7 \pm 6.6 \times 10^6$) and H (P + T) was negligible ($P > 0.05$). The morphology of erythrocytes and platelets adhered to the surface of the hydrogel was observed under SEM. As shown in Fig. S20, the typically biconcave disk shaped erythrocytes were found on the surface of fibrin glue, H (P) and H (P + T), and showed obvious aggregation on the surface of the H (P + T), unlike the monolayer adhesion of erythrocytes on the fibrin glue and H (P). Similarly, the platelets have formed irregular aggregation on the H (P) and H (P + T) surfaces, which is related to the formation of platelet plugs by activated platelets, causing accelerated blood clotting. A series of *in vitro* coagulation experiments have shown that the hydrogels, in particular H (P + T), can promote formation of blood clots, erythrocytes aggregation and platelet adhesion, thus attaining a procoagulant effect *in vitro*. Indeed, as a component of the hydrogels, the CMCS with hemostatic activity can significantly enhance the aggregation of the erythrocytes and platelets, though its mechanism in hemostasis has not been fully delineated [53, 54]. Moreover, as demonstrated by Guo's group, the catechol groups can enhance the adhesion and activation of blood cells to improve their blood-clotting capacity [55]. As ascribed to the addition of the TA, the H (P + T) was obviously better than H (P) in promoting coagulation *in vitro*, which can bind to the proteins on the cell membrane through strong hydrogen bonds and hydrophobic interactions [56]. In addition, owing to its complexation with metal ions, the TA can concentrate Ca^{2+} (i.e. blood coagulation factor IV) which is an imperative member in the coagulation cascade.

The *in vivo* hemostatic ability of the hydrogels was further explored in a rabbit model for liver injury. As illustrated in Fig. 6d, bleeding was caused by a scratch on the liver surface to simulate visceral bleeding which often occurs during surgery, and the hydrogels were used to cover the bleeding site for hemostasis. As shown in Fig. 6e, both H (P) and H (P

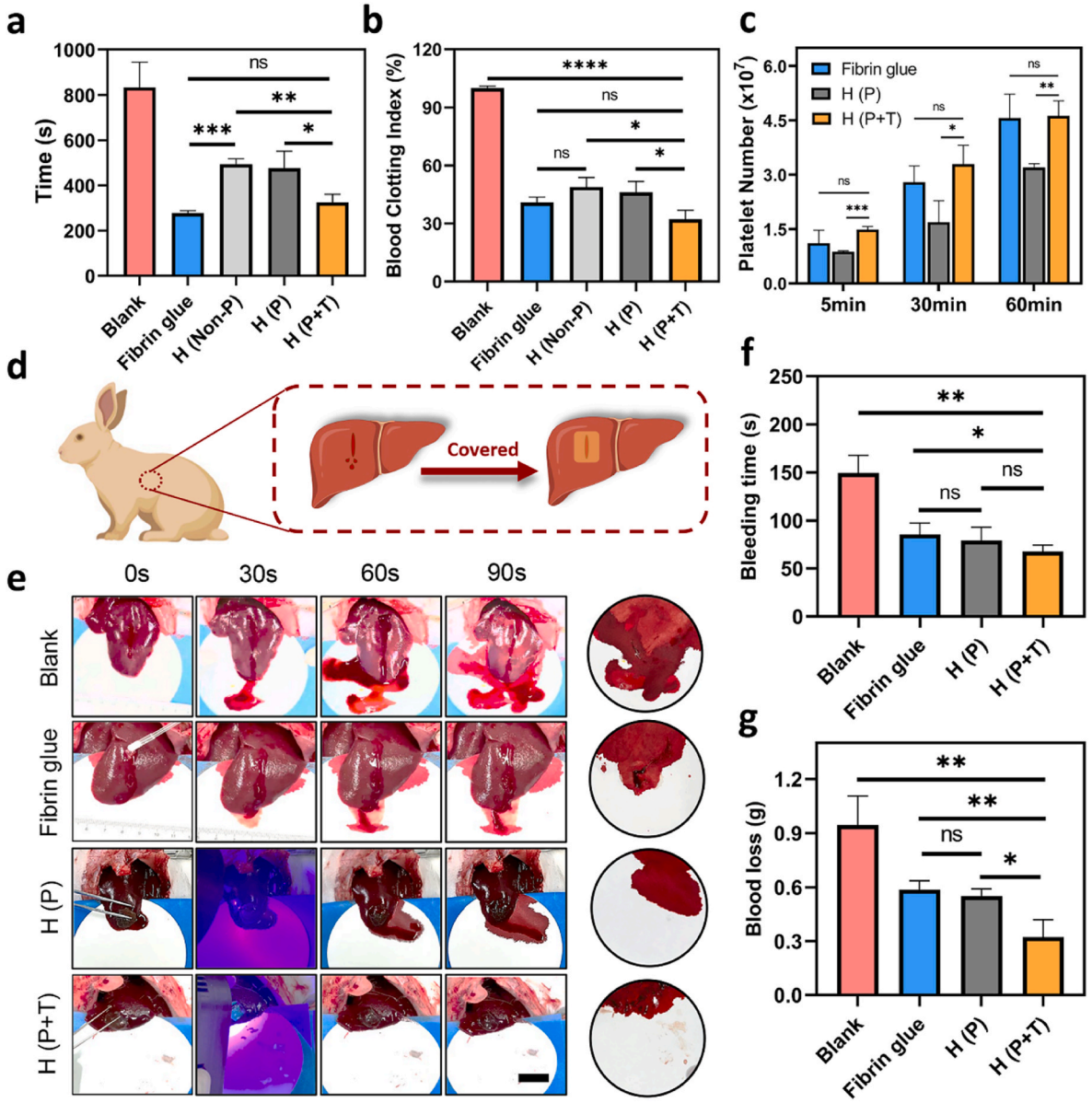

Fig. 6. a) The coagulation time of whole blood and b) BCI of fibrin glue, H (Non-P), H (P) and H (P + T) in whole blood coagulation; c) The number of adhered platelets on the surface of fibrin glue, H (P) and H (P + T) at various time points (5, 30, 60 min); d) Schematic diagram of the rabbit liver bleeding model and hydrogel hemostasis process; e) Photograph of hemostasis process (Scale bar = 2 cm), f) bleeding time and g) blood loss in various groups (*$P < 0.05$, **$P < 0.01$, ***$P < 0.001$, ****$P < 0.0001$, ns: no significant difference).

+ T) had adhered the surface of the liver even with the bleeding owing to their robust bio-adhesion. As can be seen from the blood on the filter paper, the fibrin glue, H (P) and H (P + T) were all effective in reducing the bleeding. The blood loss in the fibrin glue group (0.59 ± 0.05 g) and H (P) group (0.55 ± 0.04 g) was 1.84 times and 1.72 times that of the H (P + T) group (0.32 ± 0.10 g), respectively, indicating that the H (P + T) possesses a hemostatic potential (Fig. 6f). The bleeding time has decreased from 149.3 ± 18.3 s with no treatment (blank group) to 67.3 ± 7.0 s in the H (P + T) group, which showed a significant difference (Fig. 6g) (**$P < 0.01$). The excellent hemostatic performance of the hydrogel is attributed to the synergistic action of bio-adhesion and pro-coagulant activity. On one hand, the hydrogel has covered and adhered tightly to the bleeding area, forming a barrier which acted as a physical hemostasis. Moreover, the self-healing ability of the hydrogels is conducive to the maintenance of its integrity and bio-adhesion. On the other hand, as evidenced by *in vitro* pro-coagulant tests, both the CMCS and TA in the hydrogels promoted the aggregation and adhesion of erythrocytes and platelets to promote the formation of blood clots.

3.7. Infected wound healing of the hydrogels

An ideal tissue adhesive should not only effectively control bleeding, but also promote wound healing [16]. Considering the high rate of infection due to inadequate disinfection in the battlefield or at accidents, an infected full-thickness skin defect model was constructed to evaluate the repair effect of the H (P) and H (P + T). The commercially made pro-healing gel (EGF Gel) and antibacterial gel (Ag^+ Gel) were used as the positive controls, while PBS was used as the negative control. Wound infection and antibacterial performance of various groups were first evaluated. As shown in Figs. 7a and S21, prior to the infection, almost no colonies were found at the site of wound. However, after the infection, redness and purulency had appeared at the wound sites in all groups infected with *S. aureus*, with a large number of colonies grown in petri dishes, indicating that the wounds were heavily infected. Compared

with the PBS and EGF Gel, bacterial proliferation was significantly inhibited by the Ag^+ Gel, H (P) and H (P + T). In keeping with the results of *in vitro* antibacterial experiments, the H (P) and H (P + T) both demonstrated an outstanding antibacterial effect *in vivo*, in particular H (P + T). The viability of bacteria at the wound site was only 5.2 ± 2.7%, which was significantly lower than the Ag^+ Gel (20.9 ± 5.0%) (**P < 0.01). An active promotion of wound healing induced by the H (P) and H (P + T) was shown in Fig. 7a–c. With the elapse of time, the wound areas in all groups had gradually decreased. After 7 days of healing, the ability to pro-healing was remarkably different among the groups. The wound area of the H (P) and H (P + T) groups was much smaller compared with the other three groups. In particular, the healing rate of the H (P + T) group (77.2 ± 2.0%) was 1.78, 1.47 and 1.40 times greater than those of the PBS, EGF Gel and Ag^+ Gel groups, respectively. On the 21st day, the wounds of the H (P) and H (P + T) had almost healed completely, while the wound closure of the PBS, EGF Gel and Ag^+ Gel groups were only 87.6 ± 2.0%, 93.2 ± 0.8% and 90.4 ± 3.1%, respectively. The assay using the DHE probe also showed excellent ROS scavenging ability for the hydrogels *in vitro*. As shown in Fig. S22, on day 7, the fluorescence intensity of the H (P + T) and H (P) groups was only 19.9 ± 4.4% and 28.0 ± 5.2% that of the PBS group, and the ROS at the wound site treated by the H (P + T) and H (P) was at particularly low level during the whole process of healing, which was conducive to the reduction of inflammation and wound healing. Furthermore, the ROS scavenging efficiency at the wound site of the H (P + T) was significantly higher than that of the H (P), which was in keeping with the results of *in vitro*

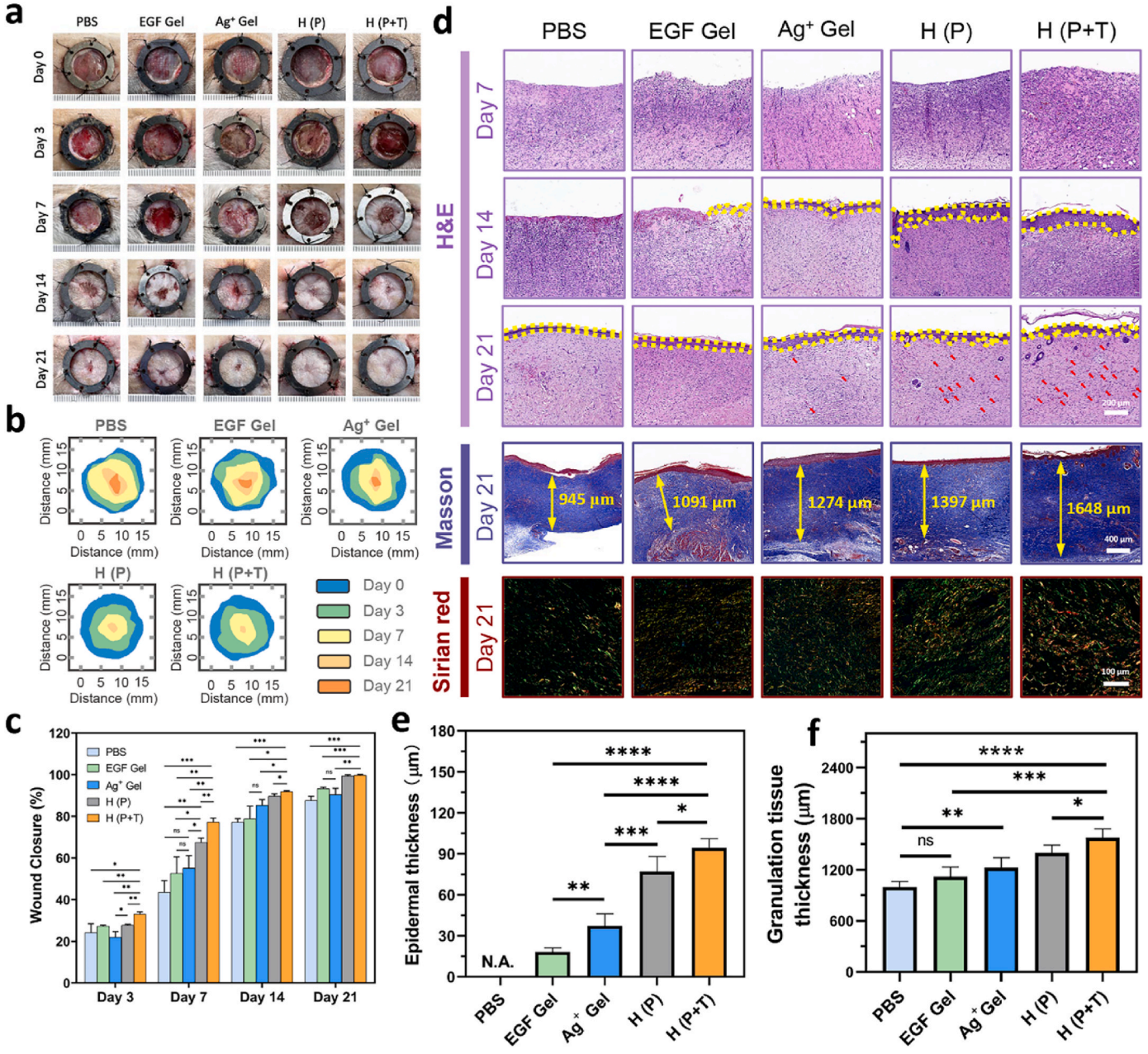

Fig. 7. a) Photographs of the wound, b) schematic diagram of the wound area, c) and closure of the wound in the PBS, EGF Gel, Ag^+ Gel, H (P) and H (P + T) groups during the healing process; d) H&E staining (Red arrow: blood vessel, Scale bar = 200 μm), Masson staining (Scale bar = 400 μm) and Sirius red staining (Scale bar = 100 μm) of various groups; e) Epithelial thickness at day 14 and f) granulation tissue thickness of various groups at day 21 (*P < 0.05, **P < 0.01, ***P < 0.001, ****P < 0.0001, ns: no significant difference). (For interpretation of the references to colour in this figure legend, the reader is referred to the Web version of this article.)

antioxidant experiments.

To further analyze the wound repair process from the histological perspective, H&E staining, Masson staining and Sirius red staining were carried out (Fig. 7d). As shown by H&E staining, re-epithelialization as a key index for the healing process has completed when the wound was covered with epithelial cells [57]. The neo-epithelium was first observed on 14th day in the EGF Gel, Ag^+ Gel, H (P) and H (P + T) groups. Among these, smooth and intact epithelium were only present in the latter three groups, whilst only discontinuous epithelium was formed in the EGF Gel group, and the H (P + T) group has shown a thicker epithelium (90 μm), indicating a more adequate re-epithelialization process (Fig. 7e). For it can provide nutrients and space for tissue remolding, many have believed that thicker granulation tissue can facilitate wound healing [58]. As shown by Masson staining, the H (P + T)-treated wound on the 21st day possessed the thickest granulation tissue (1579.4 ± 100.8 μm), whilst the EGF Gel and Ag^+ Gel measured only 1121.9 ± 108.7 μm and 1224.6 ± 116.6 μm, respectively (Fig. 7f). Collagen fibers are apt to change from type III to type I gradually [59], which can be stained as green and red/orange, respectively, by Sirius red dyes. As shown in Figs. 7d and S23, after treatment with the hydrogels, the collagen content of the wound has significantly increased, which was in keeping with the result of Masson staining, and the ratio of type I to type III collagen treated by the H (P) and H (P + T) was 1.24 and 1.37 times that of the PBS group, suggesting an earlier onset of the remodeling phase.

At the initial stage, inflammation has a great impact on wound healing, and it is generally believed that excessive immune response can hinder wound healing. Macrophages play an important role in the inflammatory stage, while decreased M1-type macrophages mark the reduction of inflammatory response. In this study, immunofluorescence staining has shown fewer M1-type macrophages ($CD86^+$) at the wound sites in the H (P) and H (P + T) compared with the other three groups after 7 days of treatment, with the relative $CD86^+$ area being 49.8 ± 4.5% and 35.3 ± 7.8%, respectively (Fig. 8a,c). Tumor necrosis factor (TNF-α), a proinflammatory cytokine produced mainly by macrophages and monocytes, was quantified with ELISA assay. As depicted in Fig. 8e, the TNF-α in H (P + T)-treated wound (18.0 ± 5.1 pg mL^{-1}) was 0.62, 0.62 and 0.63 times that of the PBS, EGF Gel and Ag^+ Gel groups, respectively. Hydrogels, in particular the H (P + T), can effectively suppress inflammation for their excellent antibacterial and antioxidant properties. The neovascularization can facilitate transportation of oxygen and nutrients to the wound site [58,60,61]. In this study, blood vessel regeneration was noted on the 21st day by CD31 immunofluorescence staining (Fig. 8b,d), and the $CD31^+$ area in the H (P + T) group (350.1 ± 35.6%) was greater than that of other groups. More capillaries and arterioles were noted in the H (P + T)-treated wound sites compared with others, which was in keeping with the result of H&E staining (Fig. 7b). Vascular endothelial growth factor (VEGF) has been implicated in vascular endothelial cell migration, proliferation and angiogenesis [62,63]. In this study, the VEGF in the H (P + T) group was 9.4 ± 1.4 pg mL^{-1}, 2.24, 1.63, 1.71 and 1.47 times higher than that in the PBS, EGF Gel, Ag^+ Gel and H (P) groups, respectively (Fig. 8f).

The efficiency of infected wound healing has differed with the treatments. EGF Gel contains epidermal growth factor (EGF) which can promote healing, but the lack of antibacterial property has attenuated its role in the healing of infected wound. Similarly, although Ag^+ Gel has certain antibacterial effect, its pro-healing effect is limited by devoid antioxidant properties and absence of pro-healing components. The SA and CMCS will not cause excessive inflammation due to their excellent biocompatibility, but will keep the wounds moist and promote fibroblast proliferation and granulation tissue formation [64,65]. Considering the inflammation, neovascularization, re-epithelialization, granulation tissue formation and collagen change, we propose that the antibacterial and antioxidative properties owned by the H (P + T) can better promote wound healing.

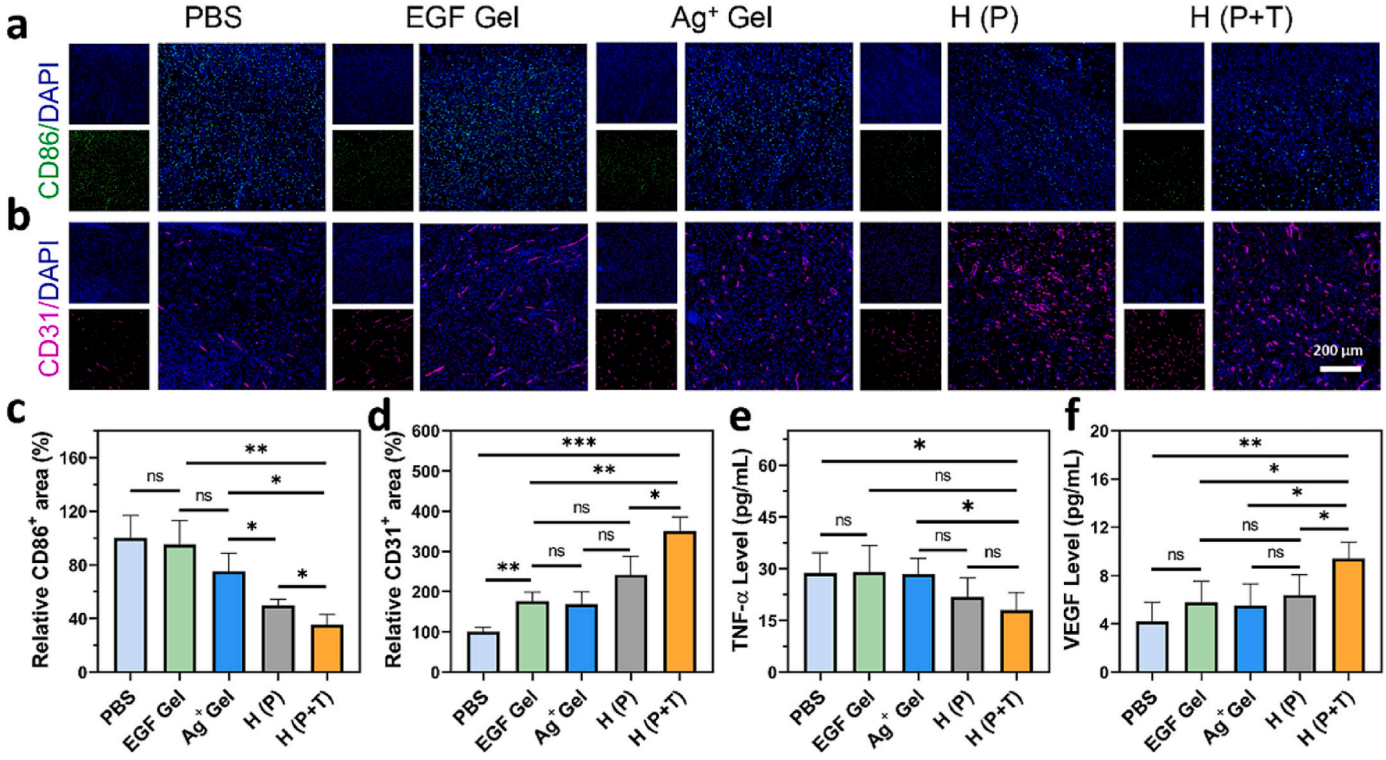

Fig. 8. a) CD86 immunofluorescence staining and c) relative $CD86^+$ area at wound of PBS, EGF Gel, Ag^+ Gel, H (P) and H (P + T) groups on the 7th day, Scale bar = 200 μm; b) CD31 immunofluorescence staining and d) relative $CD31^+$ area at wound of various groups on the 21st day, Scale bar = 200 μm; e) TNF-α and f) VEGF content in the wound sites of various groups on 7 and 21 days by ELISA assay (*$P < 0.05$, **$P < 0.01$, ***$P < 0.001$). (For interpretation of the references to colour in this figure legend, the reader is referred to the Web version of this article.)

4. Conclusion

In this study, the polysaccharide-based hydrogels with outstanding bio-adhesive, pro-coagulant, antibacterial and antioxidant properties were prepared through multi-crosslinking strategies including dynamic covalent bonds, photo-triggered covalent bonds and hydrogen bonds networks, which synergistically enhanced the mechanical properties of the hydrogels and conferred them with strength and flexibility. The considerable bio-adhesion of the hydrogels was endowed based on a mussel-inspired design and improved by the enhancement of cohesion. As the result, the adhesive strength of the H (P + T) (162.6 ± 7.0 kPa) was 12.3 times that of the fibrin glue (13.2 ± 4.9 kPa), and the self-healing properties of the H (P + T) has enabled restoration of the bio-adhesion by 83.8% after 2 h of self-healing. The excellent antibacterial and antioxidant properties of the hydrogels have been demonstrated both *in vitro* and *in vivo*. Furthermore, the hydrogels showed reliable biocompatibility and moderate degradation rate *in vivo*. For its sufficient bio-adhesion and inherent pro-coagulant activity, the H (P + T) has attained better hemostatic performance compared with the fibrin glue in a rabbit model for liver injury. The healing of the infected wound was induced by the H (P + T), which also inhibited the inflammation and promoted angiogenesis. Conceivably, the multi-crosslinking strategy may provide inspiration for the design of novel tissue adhesives, and the multi-functional H (P + T) may provide a candidate for next-generation tissue adhesives, with a wide application in the clinics for the first-aid hemostasis and infected wound healing.

Declaration of interest statement

This manuscript has been approved by all coauthors. It has not been published or presented elsewhere in part or in entirety and is not under consideration by another journal. We have read and understood your journal's policies, and we believe that neither the manuscript nor the study violates any of these. There are no conflicts of interest to declare.

CRediT authorship contribution statement

Chen-Yu Zou: Formal analysis, Methodology, Writing – original draft. **Xiong-Xin Lei:** Methodology, Formal analysis, Writing – original draft. **Juan-Juan Hu:** Methodology, Formal analysis. **Yan-Lin Jiang:** Methodology, Formal analysis. **Qian-Jin Li:** Methodology. **Yu-Ting Song:** Methodology. **Qing-Yi Zhang:** Methodology. **Jesse Li-Ling:** Formal analysis, Writing – original draft. **Hui-Qi Xie:** Conceptualization, Formal analysis, Writing – original draft, Funding acquisition.

Acknowledgement

This study has been jointly sponsored by the National Natural Science Foundation of China (Grant No. 32171351), the "1.3.5" Project for Disciplines of Excellence, West China Hospital, Sichuan University (Grant No. ZYJC18002), and Med-X Innovation Programme of Med-X Center for Materials, Sichuan University (Grant No. MCM202104). We thank Mr. Dai-Bing Luo and Shu-Guang Yan from the Analytical & Testing Center of Sichuan University for their assistance in mechanical testing and XPS analysis. Some elements in figures and schemes were created through BioRender.

Appendix A. Supplementary data

Supplementary data to this article can be found online at https://doi.org/10.1016/j.bioactmat.2022.02.034.

References

[1] C. Liu, X. Liu, C. Liu, N. Wang, H. Chen, W. Yao, G. Sun, Q. Song, W. Qiao, A highly efficient, in situ wet-adhesive dextran derivative sponge for rapid hemostasis, Biomaterials 205 (2019) 23–37, https://doi.org/10.1016/j.biomaterials.2019.03.016.

[2] Y. Huang, X. Zhao, C. Wang, J. Chen, Y. Liang, Z. Li, Y. Han, B. Guo, High-strength anti-bacterial composite cryogel for lethal noncompressible hemorrhage hemostasis: synergistic physical hemostasis and chemical hemostasis, Chem. Eng. J. 427 (2022), https://doi.org/10.1016/j.cej.2021.131977, 131977.

[3] Y. Hong, F. Zhou, Y. Hua, X. Zhang, C. Ni, D. Pan, Y. Zhang, D. Jiang, L. Yang, Q. Lin, Y. Zou, D. Yu, D.E. Arnot, X. Zou, L. Zhu, S. Zhang, H. Ouyang, A strongly adhesive hemostatic hydrogel for the repair of arterial and heart bleeds, Nat. Commun. 10 (1) (2019) 2060, https://doi.org/10.1038/s41467-019-10004-7.

[4] X.Y. He, A. Sun, T. Li, Y.J. Qian, H. Qian, Y.F. Ling, L.H. Zhang, Q.Y. Liu, T. Peng, Z. Qian, Mussel-inspired antimicrobial gelatin/chitosan tissue adhesive rapidly activated in situ by H_2O_2/ascorbic acid for infected wound closure, Carbohydr, Polym 247 (2020) 116692, https://doi.org/10.1016/j.carbpol.2020.116692.

[5] Y. Cui, Z. Huang, L. Lei, Q. Li, J. Jiang, Q. Zeng, A. Tang, H. Yang, Y. Zhang, Robust hemostatic bandages based on nanoclay electrospun membranes, Nat. Commun. 12 (1) (2021) 5922, https://doi.org/10.1038/s41467-021-26237-4.

[6] Y. Ma, J. Yao, Q. Liu, T. Han, J. Zhao, X. Ma, Y. Tong, G. Jin, K. Qu, B. Li, F. Xu, Liquid bandage harvests robust adhesive, hemostatic, and antibacterial performances as a first-aid tissue adhesive, Adv. Funct. Mater. 30 (39) (2020) 2001820, https://doi.org/10.1002/adfm.202001820.

[7] M. Li, Y. Liang, J. He, H. Zhang, B. Guo, Two-pronged strategy of biomechanically active and biochemically multifunctional hydrogel wound dressing to accelerate wound closure and wound healing, Chem. Mater. 32 (23) (2020) 9937–9953, https://doi.org/10.1021/acs.chemmater.0c02823.

[8] C. Ghobril, M.W. Grinstaff, The chemistry and engineering of polymeric hydrogel adhesives for wound closure: a tutorial, Chem. Soc. Rev. 44 (7) (2015) 1820–1835, https://doi.org/10.1039/c4cs00332b.

[9] Z. Bao, M. Gao, Y. Sun, R. Nian, M. Xian, The recent progress of tissue adhesives in design strategies, adhesive mechanism and applications, Mater. Sci. Eng. C 111 (2020) 110796, https://doi.org/10.1016/j.msec.2020.110796.

[10] L. Teng, Z. Shao, Q. Bai, X. Zhang, Y.S. He, J. Lu, D. Zou, C. Feng, C.M. Dong, Biomimetic glycopolypeptide hydrogels with tunable adhesion and microporous structure for fast hemostasis and highly efficient wound healing, Adv. Funct. Mater. 31 (43) (2021) 2105628, https://doi.org/10.1002/adfm.202105628.

[11] C. Fan, J. Fu, W. Zhu, D.A. Wang, A mussel-inspired double-crosslinked tissue adhesive intended for internal medical use, Acta Biomater. 33 (2016) 51–63, https://doi.org/10.1016/j.actbio.2016.02.003.

[12] H. Li, R. Niu, J. Yang, J. Nie, D. Yang, Photocrosslinkable tissue adhesive based on dextran, Carbohydr. Polym. 86 (4) (2011) 1578–1585, https://doi.org/10.1016/j.carbpol.2011.06.068.

[13] S. Nam, D. Mooney, Polymeric tissue adhesives, Chem. Rev. 121 (18) (2021) 11336–11384, https://doi.org/10.1021/acs.chemrev.0c00798.

[14] V. Bhagat, M.L. Becker, Degradable adhesives for surgery and tissue engineering, Biomacromolecules 18 (10) (2017) 3009–3039, https://doi.org/10.1021/acs.biomac.7b00969.

[15] N. Annabi, A. Tamayol, S.R. Shin, A.M. Ghaemmaghami, N.A. Peppas, A. Khademhosseini, Surgical materials: current challenges and nano-enabled solutions, Nano Today 9 (5) (2014) 574–589, https://doi.org/10.1016/j.nantod.2014.09.006.

[16] B. Guo, R. Dong, Y. Liang, M. Li, Haemostatic materials for wound healing applications, Nat. Rev. Chem. 5 (2021) 773–791, https://doi.org/10.1038/s41570-021-00323-z.

[17] Y. Liang, Z. Li, Y. Huang, R. Yu, B. Guo, Dual-dynamic-bond cross-linked antibacterial adhesive hydrogel sealants with on-demand removability for post-wound-closure and infected wound healing, ACS Nano 15 (4) (2021) 7078–7093, https://doi.org/10.1021/acsnano.1c00204.

[18] X. Yang, W. Liu, N. Li, M. Wang, B. Liang, I. Ullah, A. Luis Neve, Y. Feng, H. Chen, C. Shi, Design and development of polysaccharide hemostatic materials and their hemostatic mechanism, Biomater. Sci. 5 (12) (2017) 2357–2368, https://doi.org/10.1039/c7bm00554g.

[19] B.-D. Zheng, J. Ye, Y.-C. Yang, Y.-Y. Huang, M.-T. Xiao, Self-healing polysaccharide-based injectable hydrogels with antibacterial activity for wound healing, Carbohydr. Polym. 275 (2022) 118770, https://doi.org/10.1016/j.carbpol.2021.118770.

[20] J. Yang, R. Bai, B. Chen, Z. Suo, Hydrogel adhesion: a supramolecular synergy of chemistry, topology, and mechanics, Adv. Funct. Mater. 30 (2) (2019) 1901693, https://doi.org/10.1002/adfm.201901693.

[21] X. Zhao, D. Pei, Y. Yang, K. Xu, J. Yu, Y. Zhang, Q. Zhang, G. He, Y. Zhang, A. Li, Y. Cheng, X. Chen, Green tea derivative driven smart hydrogels with desired functions for chronic diabetic wound treatment, Adv. Funct. Mater. 31 (18) (2021), https://doi.org/10.1002/adfm.202009442, 2009442.

[22] A. Zhang, Y. Liu, D. Qin, M. Sun, T. Wang, X. Chen, Research status of self-healing hydrogel for wound management: a review, Int. J. Biol. Macromol. 164 (2020) 2108–2123, https://doi.org/10.1016/j.ijbiomac.2020.08.109.

[23] J. Tang, K. Xi, H. Chen, L. Wang, D. Li, Y. Xu, T. Xin, L. Wu, Y. Zhou, J. Bian, Z. Cai, H. Yang, L. Deng, Y. Gu, W. Cui, L. Chen, Flexible osteogenic glue as an All-In-One solution to assist fracture fixation and healing, Adv. Funct. Mater. 31 (38) (2021) 2102465, https://doi.org/10.1002/adfm.202102465.

[24] Y. Li, L. Yang, Y. Zeng, Y. Wu, Y. Wei, L. Tao, Self-healing hydrogel with a double dynamic network comprising Imine and Borate ester linkages, Chem. Mater. 31 (15) (2019) 5576–5583, https://doi.org/10.1021/acs.chemmater.9b01301.

[25] H. Zhao, J. Huang, Y. Li, X. Lv, H. Zhou, H. Wang, Y. Xu, C. Wang, J. Wang, Z. Liu, ROS-scavenging hydrogel to promote healing of bacteria infected diabetic wounds, Biomaterials 258 (2020) 120286, https://doi.org/10.1016/j.biomaterials.2020.120286.

[26] M. Tavakolizadeh, A. Pourjavadi, M. Ansari, H. Tebyanian, S.J. Seyyed Tabaei, M. Atarod, N. Rabiee, M. Bagherzadeh, R.S. Varma, An environmentally friendly wound dressing based on a self-healing, extensible and compressible antibacterial hydrogel, Green Chem. 23 (3) (2021) 1312–1329, https://doi.org/10.1039/d0gc02719g.

[27] L. Zhang, M. Liu, Y. Zhang, R. Pei, Recent progress of highly adhesive hydrogels as wound dressings, Biomacromolecules 21 (10) (2020) 3966–3983, https://doi.org/10.1021/acs.biomac.0c01069.

[28] W. Zhang, B. Bao, F. Jiang, Y. Zhang, R. Zhou, Y. Lu, S. Lin, Q. Lin, X. Jiang, L. Zhu, Promoting oral mucosal wound healing with a hydrogel adhesive based on a phototriggered S-nitrosylation coupling reaction, Adv. Mater. 33 (48) (2021) 2105667, https://doi.org/10.1002/adma.202105667.

[29] J.G. Leprince, W.M. Palin, M.A. Hadis, J. Devaux, G. Leloup, Progress in dimethacrylate-based dental composite technology and curing efficiency, Dent. Mater. 29 (2) (2013) 139–156, https://doi.org/10.1016/j.dental.2012.11.005.

[30] Y. Hua, H. Xia, L. Jia, J. Zhao, D. Zhao, X. Yan, Y. Zhang, S. Tang, G. Zhou, L. Zhu, Q. Lin, Ultrafast, tough, and adhesive hydrogel based on hybrid photocrosslinking for articular cartilage repair in water-filled arthroscopy, Sci. Adv. 7 (35) (2021), https://doi.org/10.1126/sciadv.abg0628 eabg0628.

[31] V.G. Muir, J.A. Burdick, Chemically modified biopolymers for the formation of biomedical hydrogels, Chem. Rev. 121 (18) (2021) 10908–10949, https://doi.org/10.1021/acs.chemrev.0c00923.

[32] L. Wang, X. Zhang, K. Yang, Y.V. Fu, T. Xu, S. Li, D. Zhang, L.N. Wang, C.S. Lee, A novel double-crosslinking-double-network design for injectable hydrogels with enhanced tissue adhesion and antibacterial capability for wound treatment, Adv. Funct. Mater. 30 (1) (2019) 1904156, https://doi.org/10.1002/adfm.201904156.

[33] M. Tavafoghi, A. Sheikhi, R. Tutar, J. Jahangiry, A. Baidya, R. Haghniaz, A. Khademhosseini, Engineering tough, injectable, naturally derived, bioadhesive composite hydrogels, Adv. Healthc. Mater. 9 (10) (2020), e1901722, https://doi.org/10.1002/adhm.201901722.

[34] N. Ninan, A. Forget, V.P. Shastri, N.H. Voelcker, A. Blencowe, Antibacterial and anti-inflammatory pH-responsive tannic acid-carboxylated agarose composite hydrogels for wound healing, ACS Appl. Mater. Interfaces 8 (42) (2016) 28511–28521, https://doi.org/10.1021/acsami.6b10491.

[35] A. Pourjavadi, M. Tavakolizadeh, S.H. Hosseini, N. Rabiee, M. Bagherzadeh, Highly stretchable, self-adhesive, and self-healable double network hydrogel based on alginate/polyacrylamide with tunable mechanical properties, J. Polym. Sci. 58 (15) (2020) 2062–2073, https://doi.org/10.1002/pol.20200295.

[36] X.Z. Zhang, Y.L. Jiang, J.G. Hu, L.M. Zhao, Q.Z. Chen, Y. Liang, Y. Zhang, X.X. Lei, R. Wang, Y. Lei, Q.Y. Zhang, J. Li-Ling, H.Q. Xie, Procyanidins-crosslinked small intestine submucosa: a bladder patch promotes smooth muscle regeneration and bladder function restoration in a rabbit model, Bioact. Mater. 6 (6) (2021) 1827–1838, https://doi.org/10.1016/j.bioactmat.2020.11.023.

[37] Y. Liang, X. Zhao, T. Hu, B. Chen, Z. Yin, P.X. Ma, B. Guo, Adhesive Hemostatic Conducting injectable composite hydrogels with sustained drug release and photothermal antibacterial activity to promote full-thickness skin regeneration during wound healing, Small 15 (12) (2019), e1900046, https://doi.org/10.1002/smll.201900046.

[38] G.M. Taboada, K. Yang, M.J.N. Pereira, S.S. Liu, Y. Hu, J.M. Karp, N. Artzi, Y. Lee, Overcoming the translational barriers of tissue adhesives, Nat. Rev. Mater. 5 (4) (2020) 310–329, https://doi.org/10.1038/s41578-019-0171-7.

[39] S. Hu, X. Pei, L. Duan, Z. Zhu, Y. Liu, J. Chen, T. Chen, P. Ji, Q. Wan, J. Wang, A mussel-inspired film for adhesion to wet buccal tissue and efficient buccal drug delivery, Nat. Commun. 12 (1) (2021) 1689, https://doi.org/10.1038/s41467-021-21989-5.

[40] T. Priemel, G. Palia, F. Förste, F. Jehle, S. Sviben, I. Mantouvalou, P. Zaslansky, L. Bertinetti, M.J. Harrington, Microfluidic-like fabrication of metal ion-cured bioadhesives by mussels, Science 374 (6564) (2021) 206–211, https://doi.org/10.1126/science.abi9702.

[41] A. Bal-Ozturk, B. Cecen, M. Avci-Adali, S.N. Topkaya, E. Alarcin, G. Yasayan, Y. C. Ethan, B. Bulkurcuoglu, A. Akpek, H. Avci, K. Shi, S.R. Shin, S. Hassan, Tissue adhesives: from research to clinical translation, Nano Today 36 (2021) 101049, https://doi.org/10.1016/j.nantod.2020.101049.

[42] K. Zhang, X. Chen, Y. Xue, J. Lin, X. Liang, J. Zhang, J. Zhang, G. Chen, C. Cai, J. Liu, Tough hydrogel bioadhesives for sutureless wound sealing, hemostasis and biointerfaces, Adv. Funct. Mater. (2021) 2111465, https://doi.org/10.1002/adfm.202111465.

[43] L. Zhou, H. Zheng, Z. Liu, S. Wang, Z. Liu, F. Chen, H. Zhang, J. Kong, F. Zhou, Q. Zhang, Conductive antibacterial hemostatic multifunctional scaffolds based on $Ti_3C_2T_x$ MXene nanosheets for promoting multidrug-resistant bacteria-infected wound healing, ACS Nano 15 (2) (2021) 2468–2480, https://doi.org/10.1021/acsnano.0c06287.

[44] P.A. Mouthuy, S.J.B. Snelling, S.G. Dakin, L. Milkovic, A.C. Gasparovic, A.J. Carr, N. Zarkovic, Biocompatibility of implantable materials: an oxidative stress viewpoint, Biomaterials 109 (2016) 55–68, https://doi.org/10.1016/j.biomaterials.2016.09.010.

[45] J. Li, S. Zhuang, Antibacterial activity of chitosan and its derivatives and their interaction mechanism with bacteria: current state and perspectives, Eur. Polym. J. 138 (2020) 109984, https://doi.org/10.1016/j.eurpolymj.2020.109984.

[46] X. He, X. Liu, J. Yang, H. Du, N. Chai, Z. Sha, M. Geng, X. Zhou, C. He, Tannic acid-reinforced methacrylated chitosan/methacrylated silk fibroin hydrogels with multifunctionality for accelerating wound healing, Carbohydr. Polym. 247 (2020) 116689, https://doi.org/10.1016/j.carbpol.2020.116689.

[47] O.P.N. Yarley, A.B. Kojo, C. Zhou, X. Yu, A. Gideon, H.H. Kwadwo, O. Richard, Reviews on mechanisms of in vitro antioxidant, antibacterial and anticancer activities of water-soluble plant polysaccharides, Int. J. Biol. Macromol. 183 (2021) 2262–2271, https://doi.org/10.1016/j.ijbiomac.2021.05.181.

[48] N. Nikfarjam, M. Ghomi, T. Agarwal, M. Hassanpour, E. Sharifi, D. Khorsandi, M. Ali Khan, F. Rossi, A. Rossetti, E. Nazarzadeh Zare, N. Rabiee, D. Afshar, M. Vosough, T. Kumar Maiti, V. Mattoli, E. Lichtfouse, F.R. Tay, P. Makvandi, Antimicrobial ionic liquid-based materials for biomedical applications, Adv. Funct. Mater. 31 (42) (2021) 2104148, https://doi.org/10.1002/adfm.202104148.

[49] Y. Fu, J. Zhang, Y. Wang, J. Li, J. Bao, X. Xu, C. Zhang, Y. Li, H. Wu, Z. Gu, Reduced polydopamine nanoparticles incorporated oxidized dextran/chitosan hybrid hydrogels with enhanced antioxidative and antibacterial properties for accelerated wound healing, Carbohydr. Polym. 257 (2021) 117598, https://doi.org/10.1016/j.carbpol.2020.117598.

[50] J. Tan, Q.Y. Zhang, L.P. Huang, K. Huang, H.Q. Xie, Decellularized scaffold and its elicited immune response towards the host: the underlying mechanism and means of immunomodulatory modification, Biomater. Sci. 9 (14) (2021) 4803–4820, https://doi.org/10.1039/d1bm00470k.

[51] J. Huang, Y. Jiang, Y. Liu, Y. Ren, Z. Xu, Z. Li, Y. Zhao, X. Wu, J. Ren, Marine-inspired molecular mimicry generates a drug-free, but immunogenic hydrogel adhesive protecting surgical anastomosis, Bioact. Mater. 6 (3) (2021) 770–782, https://doi.org/10.1016/j.bioactmat.2020.09.010.

[52] D.C. Roy, N.A. Mooney, C.H. Raeman, D. Dalecki, D.C. Hocking, Fibronectin matrix mimetics promote full-thickness wound repair in diabetic mice, Tissue Eng. 19 (21–22) (2013) 2517–2526, https://doi.org/10.1089/ten.TEA.2013.0024.

[53] I. Koumentakou, Z. Terzopoulou, A. Michopoulou, I. Kalafatakis, K. Theodorakis, D. Tzetzis, D. Bikiaris, Chitosan dressings containing inorganic additives and levofloxacin as potential wound care products with enhanced hemostatic properties, Int. J. Biol. Macromol. 162 (2020) 693–703, https://doi.org/10.1016/j.ijbiomac.2020.06.187.

[54] J. Li, X. Sun, K. Zhang, G. Yang, Y. Mu, C. Su, J. Pang, T. Chen, X. Chen, C. Feng, Chitosan/Diatom-biosilica aerogel with controlled porous structure for rapid hemostasis, Adv. Healthc. Mater. 9 (21) (2020), e2000951, https://doi.org/10.1002/adhm.202000951.

[55] Y. Huang, X. Zhao, Z. Zhang, Y. Liang, Z. Yin, B. Chen, L. Bai, Y. Han, B. Guo, Degradable gelatin-based IPN cryogel hemostat for rapidly stopping deep noncompressible hemorrhage and simultaneously improving wound healing, Chem. Mater. 32 (15) (2020) 6595–6610, https://doi.org/10.1021/acs.chemmater.0c02030.

[56] L. Deng, Y. Qi, Z. Liu, Y. Xi, W. Xue, Effect of tannic acid on blood components and functions, Colloids Surf., B 184 (2019) 110505, https://doi.org/10.1016/j.colsurfb.2019.110505.

[57] J. Qu, X. Zhao, Y. Liang, Y. Xu, P.X. Ma, B. Guo, Degradable conductive injectable hydrogels as novel antibacterial, anti-oxidant wound dressings for wound healing, Chem. Eng. J. 362 (2019) 548–560, https://doi.org/10.1016/j.cej.2019.01.028.

[58] Y. Liang, J. He, B. Guo, Functional hydrogels as wound dressing to enhance wound healing, ACS Nano 15 (8) (2021) 12687–12722, https://doi.org/10.1021/acsnano.1c04206.

[59] X. Tang, X. Wang, Y. Sun, L. Zhao, D. Li, J. Zhang, H. Sun, B. Yang, Magnesium oxide-assisted dual-cross-linking bio-multifunctional hydrogels for wound repair during full-thickness skin injuries, Adv. Funct. Mater. 31 (43) (2021) 2105718, https://doi.org/10.1002/adfm.202105718.

[60] Z. Tu, M. Chen, M. Wang, Z. Shao, X. Jiang, K. Wang, Z. Yao, S. Yang, X. Zhang, W. Gao, C. Lin, B. Lei, C. Mao, Engineering bioactive M2 macrophage-polarized anti-inflammatory, antioxidant, and antibacterial scaffolds for rapid angiogenesis and diabetic wound repair, Adv. Funct. Mater. 31 (30) (2021), https://doi.org/10.1002/adfm.202100924, 2100924.

[61] G. Cao, Y. Huang, K. Li, Y. Fan, H. Xie, X. Li, Small intestinal submucosa: superiority, limitations and solutions, and its potential to address bottlenecks in tissue repair, J. Mater. Chem. B 7 (33) (2019) 5038–5055, https://doi.org/10.1039/c9tb00530g.

[62] H. Ma, Q. Zhou, J. Chang, C. Wu, Grape seed-inspired smart hydrogel scaffolds for melanoma therapy and wound healing, ACS Nano 13 (4) (2019) 4302–4311, https://doi.org/10.1021/acsnano.8b09496.

[63] S. Nour, N. Baheiraei, R. Imani, M. Khodaei, A. Alizadeh, N. Rabiee, S.M. Moazzeni, A review of accelerated wound healing approaches: biomaterial- assisted tissue remodeling, J. Mater. Sci. Mater. Med. 30 (10) (2019) 120, https://doi.org/10.1007/s10856-019-6319-6.

[64] Z. Zhai, K. Xu, L. Mei, C. Wu, J. Liu, Z. Liu, L. Wan, W. Zhong, Co-assembled supramolecular hydrogels of cell adhesive peptide and alginate for rapid hemostasis and efficacious wound healing, Soft Matter 15 (42) (2019) 8603–8610, https://doi.org/10.1039/c9sm01296f.

[65] Z. Luo, K. Xue, X. Zhang, J.Y.C. Lim, X. Lai, D.J. Young, Z.X. Zhang, Y.L. Wu, X. J. Loh, Thermogelling chitosan-based polymers for the treatment of oral mucosa ulcers, Biomater. Sci. 8 (5) (2020) 1364–1379, https://doi.org/10.1039/c9bm01754b.